Since January 2020 Elsevier has created a COVID-19 resource centre with free information in English and Mandarin on the novel coronavirus COVID-19. The COVID-19 resource centre is hosted on Elsevier Connect, the company's public news and information website.

Bioorganic Chemistry 105 (2020) 104357

Contents lists available at ScienceDirect

Bioorganic Chemistry

journal homepage: www.elsevier.com/locate/bioorg

Design and synthesis of thiadiazolo-carboxamide bridged β-carboline-indole hybrids: DNA intercalative topo-IIα inhibition with promising antiproliferative activity

Ramya Tokala [a], Sravani Sana [a], Uppu Jaya Lakshmi [a], Prasanthi Sankarana [a], Dilep Kumar Sigalapalli [a], Nikhil Gadewal [b], Jyoti Kode [c,d], Nagula Shankaraiah [a,*]

[a] Department of Medicinal Chemistry, National Institute of Pharmaceutical Education and Research (NIPER), Hyderabad 500 037, India
[b] Bioinformatics Centre, Advanced Centre for Treatment, Research & Education in Cancer, Tata Memorial Centre, Kharghar, Navi Mumbai 410210, India
[c] Tumor Immunology & Immunotherapy Group, Advanced Centre for Treatment, Research & Education in Cancer, Tata Memorial Centre, Kharghar, Navi Mumbai 410210, India
[d] Homi-Bhabha National Institute (HBNI), Training School Complex, Anushakti Nagar, Mumbai 400094, India

ARTICLE INFO

Keywords:
β-Carboline
Thiadiazole
DNA intercalation
Topo-IIα inhibitors
Apoptosis
Cytotoxicity

ABSTRACT

The conjoining of salient pharmacophoric properties directing the development of prominent cytotoxic agents was executed by constructing thiadiazolo-carboxamide bridged β-carboline-indole hybrids. On the evaluation of *in vitro* cytotoxic potential, **12c** exhibited prodigious cytotoxicity among the synthesized new molecules **12a**–**k**, with an IC_{50} < 5 μM in all the tested cancer cell lines (A549, MDA-MB-231, BT-474, HCT-116, THP-1) and the best cytotoxic potential was expressed in lung cancer cell line (A549) with an IC_{50} value of 2.82 ± 0.10 μM. Besides, another compound **12a** also displayed impressive cytotoxicity against A549 cell line (IC_{50}: 3.00 ± 1.40 μM). Further target-based assay of these two compounds **12c** and **12a** revealed their potential as DNA intercalative topoisomerase-IIα inhibitors. Additionally, the antiproliferative activity of compound **12c** was measured in A549 cells by traditional apoptosis assays revealing the nuclear, morphological alterations, and depolarization of membrane potential in mitochondria and externalization of phosphatidylserine in a concentration-dependent manner. Cell cycle analysis unveiled the G0/G1 phase inhibition and wound healing assay inferred the inhibition of *in vitro* cell migration by compound **12c** in lung cancer cells. Remarkably, the safety profile of compound **12c** was disclosed by screening against normal human lung epithelial cell line (BEAS-2B: IC_{50}: 71.2 ± 7.95 μM) with a selectivity index range of 14.9–25.26. Moreover, Molecular modeling studies affirm the intercalative binding of compound **12c** and **12a** in the active pocket of topo-IIα. Furthermore, *in silico* prediction of physico-chemical parameters divulged the propitious drug-like properties of the synthesized derivatives.

1. Introduction

Promising anticancer agents should be necessarily developed as cancer remains as public health concern worldwide [1] along with the additional origin of a newer pandemic like COVID-19 [2]. The drug repurposing strategy has been employed to reduce COVID-19 induced inflammation, coagulopathy and dysfunction by using anticancer agents like interleukin inhibitors, corticosteroids, kinase inhibitors, etc [2c]. The types, mutations [3], metastasis [4], resistance [5], and after-effects of clinical treatment, make it a gruesome disease [6] without ideal treatment. Consequently, there lies a lacuna in the progression of novel agents to combat cancer. Inhibition of more than one target with a key role in cell replication and proliferation set forth magnificent directions in the generation of new chemical entities (NCEs) towards chemical research.

The discovery and comprehension of the structure and function of DNA are paramount of all the discoveries in the last century [7]. Hitherto, DNA is a major pharmacological target for small molecules which are effective in various ailments which originated from virus [8], bacteria [9] and also in cancer [10]. Based on the interaction of the small molecules with DNA, they have been broadly divided into (i) Covalent inhibitors, which are irreversible binders that form covalent adducts, thereby cause serious damage to the DNA process and induce cell death. e.g., cisplatin (ii) Non-covalent inhibitors are reversible binders; further

* Corresponding author.
E-mail addresses: shankar@niperhyd.ac.in, shankar.niperhyd@gov.in (N. Shankaraiah).

https://doi.org/10.1016/j.bioorg.2020.104357
Received 29 June 2020; Received in revised form 3 September 2020; Accepted 5 October 2020
Available online 8 October 2020

classified based on modes of binding with duplex DNA, (a) Surface binders (exhibits electrostatic interactions) (b) Intercalators (between DNA base pairs) (c) Groove binders (major and minor groove binding) [11]. Usually, the small molecules bind with DNA with more than one binding mode. Also, enzymes acting on DNA play a promising role in replication and repair. One such enzyme is DNA Topoisomerase II (Topo II), with a potential role in cell division and demarcation by causing nicking and relegation of DNA and is an imperative target in drug discovery [12]. There are two isoforms of Topo II with gene codes Topo IIα and Topo IIβ which are analogous in structure and are uniform in catalytic properties. However, topo IIα has positive coordination on the mitotic process of cells such as rate of cell proliferation, expression of mRNA, and also on different phases of the cell cycle nevertheless, cellular functions of topo IIβ are yet unclear [13]. Topo II, in general, modifies DNA topology and induces double-strand breaks through multiple steps that require ATP hydrolysis and Mg^{2+} for activity [14a] and agents inhibiting it are categorized into interfacial poisons (IFPs) and catalytic inhibitory compounds (CICs). Anticancer agents like doxorubicin and etoposide are renowned Topo II poisons that cause accretion of deplorable linear DNA by inhibition of the relegation of cleaved DNA strands through the stabilization of the Topo-DNA complex. Catalytic inhibitors such as novobiocin and merbarone, block binding and nicking of DNA respectively. On the contrary, agents such as suramin, a potent catalytic inhibitor block topo II's ATP binding site [14]. In addition to the above features, agents that induce apoptosis are considered as remarkable anticancer agents as they target an important hallmark of cancer [15]. Thus the discovery of new chemical entities targeting topo II through DNA intercalation is an important area of cancer research. Based on the literature, the rationale to exhibit intercalative topo II inhibition by NCE's is to possess a chromophore (head part) linked to a side chain (tail part) through a cationic species. The mechanistic details indicate that the chromophore is a polyaromatic ring system which intercalates between DNA base pairs. The linker and extending heterocycles impart stabilization by interacting with phosphate groups and by orienting into the groove of DNA respectively [16].

The structural features of naturally occurring β-carboline alkaloids make it a potential chromophore to intercalate with DNA in between the base pairs. The tricyclic pyrido [3,4-*b*] ring system (norharmane **A**) possesses an affinity to stack between GC residues of DNA [17]. Furthermore, these *Peganum harmala* derived agents (harmine **B**) followed up by their chemical functionalization were reported as DNA damaging and photocleavage agents [18]. In synergism, inhibitions of other enzymes like topoisomerases [12,19], kinases [20] make β-carboline a promising entity in cancer research along with indications in several diseases [21].

1,3,4-Thiadiazole is another privileged heterocyclic scaffold with excellent therapeutic potential against diverse health problems. The potential of this bioactive scaffold was far recognized as an antiepileptic (acetazolamide **C**), antibacterial, antiprotozoal (megazol **D**), and to treat glaucoma [22]. Farooqi *et al.,* revealed the affinity of 1,3,4-thiadiazole towards DNA interaction by hybridization of 1,3,4-thiadiazole to the clinical drugs (Ibuprofen and Ciprofloxacin)[23]. Plech *et. al.*, proved the affinity of 1, 3, 4-thiadiazole towards topo II by disubstitution on the heterocycles [24]. Indeed, this entity reveals wide pharmacological activities such as antimicrobial, antitubercular, anti-inflammatory, antiviral, anticonvulsant, and activity against central nervous system (CNS) disorders, cardiovascular system (CVS) diseases and cancer [22].

Indole is a versatile and privileged scaffold with an extensive range of biological actions principally in cancer by targeting diverse enzymes (Topoisomerases, Tubulin polymerases, Aromatase) pathways (NF-kB/mTOR/PI3K/AKT), and mechanisms like DNA binding and apoptosis [25]. Naturally occurring antitumor antibiotic like duocarmycin has a strong affinity for DNA interaction, nonetheless unable to reach the clinic. However, synthetic analogs like adozelesin with substitution on 2nd position (**E**) reached clinical trials in the treatment of cancer. Highly effective D-64131(**F**) and D 68144 (**G**) were recognized as potent anticancer agents even in paclitaxel-resistant tumors [26] (Fig. 1).

2. Rationale

In maintaining our persistence to achieve the goal of reaching successful clinical candidates towards cancer [27], by considering the advantage of structural features of the chemically diverse scaffolds like β-carboline, 1,3,4-thiadiazole, indole and exploiting pharmacophore hybridization to carboxamide formation, we have methodologically designed a new series (**12a**–**k**) of DNA intercalative topo II inhibitors with classical apoptosis-inducing features. The rationale for this design has been established based on literature and structural functionalities as illustrated in Fig. 2. Foremost requirements for intercalative topoisomerase II inhibition are the presence of a chromophore (intercalation into DNA), adjoining cationic center (electrostatic interaction with base pairs), and a groove extending side-chain/heterocycles (stabilization). DNA intercalative topoisomerase II inhibitors such as doxorubicin and PD-115934 also possess this kind of arrangement (chromophore + cationic center + groove extending side chain) [16] and support the rationale to this design. The chemical synthesis of β-carboline acid from amino acid L-tryptophan satisfies the utmost feature as a chromophore for dual activity. Further, the cationic center of 1,3,4-thiadiazole on the 2nd position of indole (extending heterocycles) has been constructed by utilizing chemical functionalities of indole-2-acid and thiosemicarbazide followed by cyclization resulting in the free amino moiety. The chromophore has been adjoined with the rest of the scaffold by pharmacophore hybridization [28] *via* carboxamide formation through acid amine coupling.

3. Chemistry

The desired hybrids 1,3,4-thiadiazolo carboxamide bridged β-carboline-indole hybrids **12a**–**k** were synthesized *via* amide formation between β-carboline acid and indol-2-yl-1,3,4-thiadiazol-2-amine as depicted in Scheme 2. 1-Aryl-9*H*-pyrido[3,4-*b*] indole-3-carboxylic acids **6a**–**f** were synthesized by earlier reported procedures, [12] from commercially available L-tryptophan (Spectrochem; CAS NO: 73-22-3) **1** which was esterified **2** and subjected to Pictet-Spengler condensation using acid catalyst trifluoroacetic acid with substituted aromatic benzaldehydes **3a**–**f** to obtain tetrahydro-β-carboline esters **4a**–**f**. The β-carboline esters **5a**–**f** were obtained by further aromatization of **4a**–**f** using $KMnO_4$ and were subjected to basic hydrolysis to yield the respective β-carboline acids **6a**–**f** (Scheme 1).

The amine components **11a**–**c** were attained by esterification of

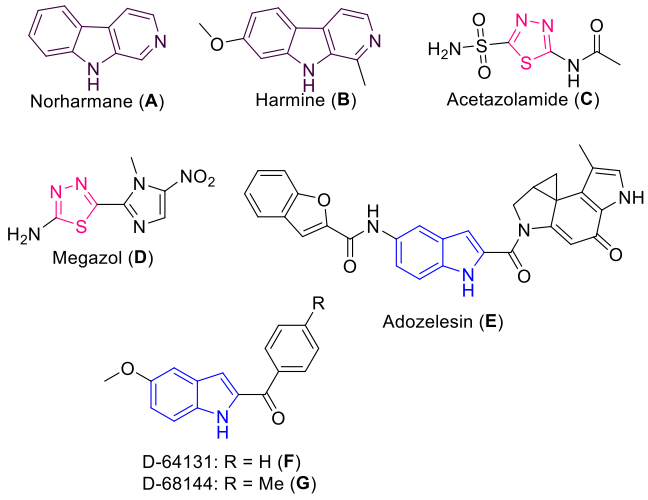

Fig. 1. Representative structures bearing pharmacologically active β-carbolines, thiadiazole, and indole nucleus.

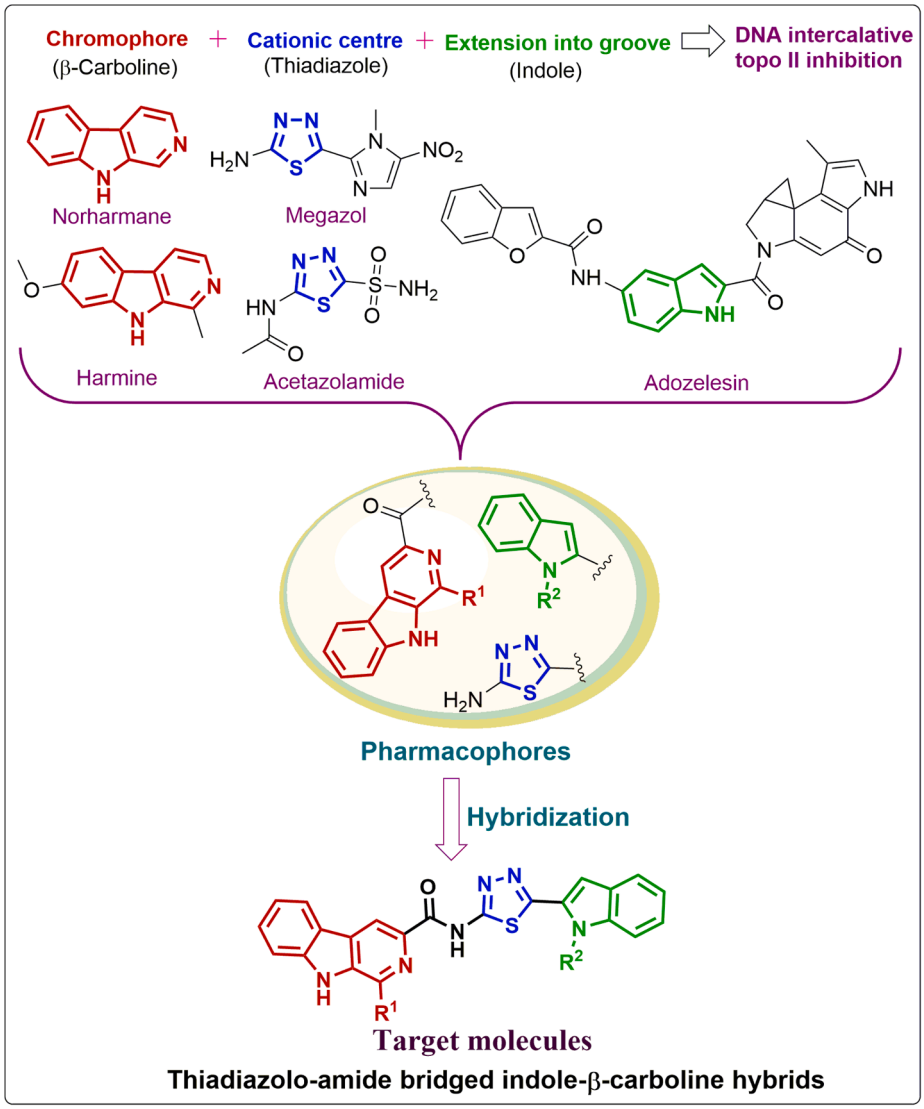

Fig. 2. Rationale in the design of target molecules (thiadiazolo-carboxamide bridged β-carboline-indole derivatives **12a**–**k**).

indole-2-acid **7**, which (**8**) was further alkylated using different alkyl halides to yield alkylated indole-2-esters **9a**–**c**. Thus obtained esters, on basic hydrolysis result in respective alkylated indole-2-acids **10a**–**c**. This acid component undergoes cyclization with thiosemicarbazide in $POCl_3$ to succumb amine counterpart. Further, the title compounds **12a**–**k** was achieved by acid–amine coupling between **6a**–**f** and **11a**–**c** in good yields (Scheme 2). All these compounds were purified by using column chromatography.

The representative compound **12a** of synthesized derivatives was thus characterized by ^{1}H NMR spectroscopy. The appearance of singlet at $\delta = 12.14$ corresponds to the amidic N—H proton and confirms the formation of titled compounds. The two singlets at $\delta = 12.58$ and 12.19 ppm account for the NH proton of indole and 9*H*-indolic proton of β-carboline ring respectively. The proton at the C4 position of β-carboline appeared as a singlet at $\delta = 9.13$ ppm. All the other 14 aromatic protons of both β-carboline and indole are accounted for in the range of $\delta = 8.55$ to 7.13 ppm. Further analysis by ^{13}C NMR spectroscopy disclosed that amidic carbonyl carbon resonated at $\delta = 164.1$ ppm. The signals at $\delta = 158.2$ and 158.0 ppm account for amide attached *C*2 carbon and indole attached C5 carbon of 1,3,4-thiadiazole respectively. All the remaining carbons of **12a** appeared in the region of $\delta =$ 142.1–104.5 ppm. Next, IR spectra show the band at 1673 cm^{-1} which indicates the C═O stretching of the amide of the compound **12a**. The HRMS exhibited specific $[M+H]^+$ peaks that matched with their molecular formula. Similarly, spectral data (^{1}H, ^{13}C, FT-IR) of all the remaining compounds **12b**–**k** matched accurately with their respective structures.

4. Biological evaluation

4.1. In vitro cytotoxicity assay

Thus, the synthesized compounds **12a**–**k** were evaluated for their cytotoxic potential against a panel of human cancer cell lines and compared with the standard harmine and doxorubicin, VP-16 (etoposide) and represented in Table 1. The MTT [3-(4,5-dimethylthiazol-2-yl)-2,5-diphenyltetrazolium bromide] assay [29a] was performed for all the derivatives on different cancer cell lines such as (i) adherent cell lines viz lung cancer (A549), breast cancer (MDA-MB-231, BT-474), colon cancer (HCT-116), and (ii) suspension cell lines *viz* leukemia (HL-60) and acute monocytic leukemia (THP-1) (**Figs. S1 and S2** of **ESI**) and compared to normal human cell line (BEAS-2B). Notably, all the tested compounds exhibited potent cytotoxicity against all the tested cell lines, particularly **12c** with the highest cytotoxic potential of IC_{50} of 2.82 ± 0.10 μM in the A549 cell line. Further, it has leading cytotoxicity in all the cell lines tested with an IC_{50} of 3.18 ± 0.49 μM and 3.83 ± 0.94

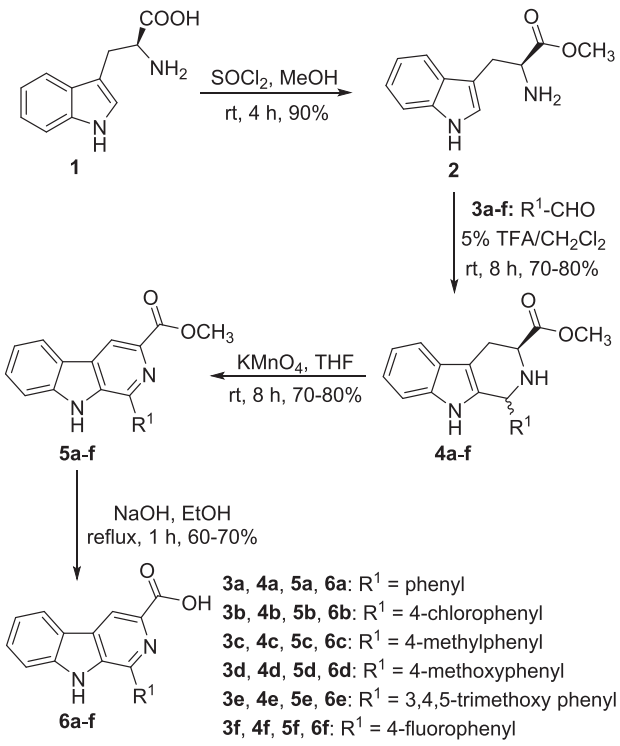

Scheme 1. Synthesis of β-carboline component **6a**–**f** (1-aryl-9*H*-pyrido[3,4-*b*] indole-3-carboxylic acids).

μM in THP-1 and HL-60 respectively. Also, in both breast cancer cell lines, **12c** expressed an IC_{50} of 3.28 ± 0.43 μM and 4.09 ± 0.59 μM in MDA-MB-231 (triple-negative) and BT-474. Also, the compound **12c** has exhibited *in vitro* cytotoxicity in HCT-116 with an IC_{50} value of 4.78 ± 1.29 μM and the order of cytotoxicity for compound **12c** in different cell lines is A549 > THP-1 > MDA-MB-231 > HL-60 > BT-474 > HCT-116.

Encouragingly, the compound **12c** displayed the lowest *in vitro* cytotoxicity with an IC_{50} value of 71.25 ± 7.95 μM in normal human lung epithelial cells (BEAS-2B). Remarkably, the compounds **12a**, **12f**, **12h**, and **12j** exhibited notable cytotoxicity potential in all the cell lines tested with overall $IC_{50} \leq 10$ μM. Moreover, compounds **12b**, **12d**, **12i**, and **12k** also expressed a reasonable *in vitro* cytotoxicity on A549 and MDA-MB-231 cell lines with an IC_{50} value < 10 μM. From the detailed analysis of the *in vitro* cytotoxicity table, it was comprehended that **12c** is a potent compound and possesses the least inhibition in BEAS-2B and the cytospecificity profile on all the human cancer cell lines along with normal human cell line was represented in graphical form in Fig. 3a.

4.2. Selectivity index

After contemplating the specificity exhibited by potent compound **12c** in different cancer cell lines and normal human cell line (Fig. 3a), the selectivity index (SI) was calculated and portrayed in Fig. 3b. The selectivity index is the ratio of IC_{50} in the non-tumor cell line to IC_{50} in the tumor cell line [29b] and a compound is said to be selective only if the value of SI ≥ 10 [29c]. It was observed that compound **12c** exhibited selectivity in all the cell lines tested with selectivity range of 25.26–14.90 in the following order A549 > THP-1 > MDA-MB-231 > HL-60 > BT-474 > HCT-116.

4.3. Structure-Activity Relationship (SAR)

Based on the established *in vitro* cytotoxicity data against human cancer cell lines, the structure–activity relationship (SAR) was constructed to provide insights regarding the pattern of efficiency of the synthesized NCEs as illustrated in Fig. 4. Two-point diverse modifications have been performed on the C1-phenyl of the β-carboline (R^1) and nitrogen of indole (R^2). Noticeably, the compounds **12a**, **12c**, **12h**, and **12j** without substitution on indole (R^2 = H) were found to be potent than substituted derivatives **12b**, **12d–g**, **12i**, and **12k**. Additionally, increase in length of alky chain (R^2 = H > Me > Et) on indole resulted in derivatives with lower cytotoxicity potential (**12c** > **12d** > **12e** & **12a** > **12b**). The better cytotoxicity was observed when R^1 is substituted by electron-donating group (EDG) (**12c–g**, **12k**: R^1 = 4-Me, 4-OMe & 3,4,5-triOMe) than no substitution (**12a**, **b**: R^1 = H) and followed by electron-withdrawing group (EWG) (**12h–j**: R^1 = 4-F & 4-Cl). The *in vitro* cytotoxic potential was compared with EDG and EWG in the following order: (**a**) **EDG**: (**i**) In derivatives where R^2 = methyl; and R^1 is 3,4,5-trimethoxy substituted, such derivative exhibited superior inhibition than 4-methoxy containing corresponding derivative (**12f** > **12d**); (**ii**) In compounds with R^2 = ethyl; the compound with 4-methyl substitution on R^1 displayed better inhibition than derivative with 3,4,5-trimethoxy followed by 4-methoxy substituted compound (**12k>12g** > **12e**); (**b**) **EWG**: In compounds with R^2 = H; the derivative with 4-chloro substitution at R^1 position exhibited higher inhibition than 4-fluoro substituted derivative (**12j** > **12h**). Interestingly, a similar pattern of inhibition was observed for all the compounds in the tested cell lines.

5. Target-based assays

5.1. Topoisomerase IIα inhibition

Topoisomerase IIα is located in the nucleus and functions as a DNA nick inducing enzyme with established importance in DNA replication. It induces nicks on both the DNA strands, religates the phosphodiester bonds, and thereby alters the DNA topology. Thus, inhibition of topoisomerase IIα results in either blockage of the enzyme to induce nicks which thereby interferes the cell replication process (CICs) or prevent the relegation of nicks caused by the enzyme by stabilization of DNA-ternary complex which results in the initiation of recombination pathways (IFPs) and ultimately results in cell death [30]. Topo-IIα inhibitory assay has been performed using Topo-IIα drug screening kit (TG1019-1, TopoGEN, USA) with enzyme human topoisomerase IIα (TG2000H-2, TopoGEN, USA). In this assay, the two most potent compounds **12c** and **12a** from IC_{50} data were evaluated for their topo-IIα inhibitory activity. The catenated kDNA and topo II (5 units) along with compound **12c** (10 μM) and **12a** (10 μM) (lane 1 and 2 respectively) didn't result in the formation of any linear DNA (**a** & **b**). Further, decatenated kDNA and linear DNA in lines 3 and 4 were the reference markers provided with the screening kit. From Fig. 5, it is evident that the compound **12c** and **12a** inhibited topo IIα to induce nicks and linearize kDNA and fall into the category of catalytic inhibitory compounds.

5.2. DNA intercalation assays

Intercalation of the ligand into DNA doesn't always cause alterations in hydrogen bonds between base pairs, but the ligand-DNA complex is stabilized by van der Waals, charge transfer, π-π stacking with the planar scaffold, hydrophobic and hydrogen-bonding interactions [31]. Intercalation stiffens, lengthens, reduces helical twist, and unwinds the DNA double helix [32], thereby resulting in inhibition of cell proliferation and triggers cell death. [33] Among various classes of DNA binding agents, intercalating agents were widely studied by considering different biophysical assays. By relating absorbance and viscosity measurements using CT-DNA with a concentration of the tested compound, these assays suggest the mode of binding of the novel synthesized compounds.

5.2.1. Relative viscosity experiment

To understand the binding mode of newly synthesized series, a relative viscosity experiment has been performed for potent compounds **12c** and **12a** using CT-DNA as per the reported protocol [34]. The

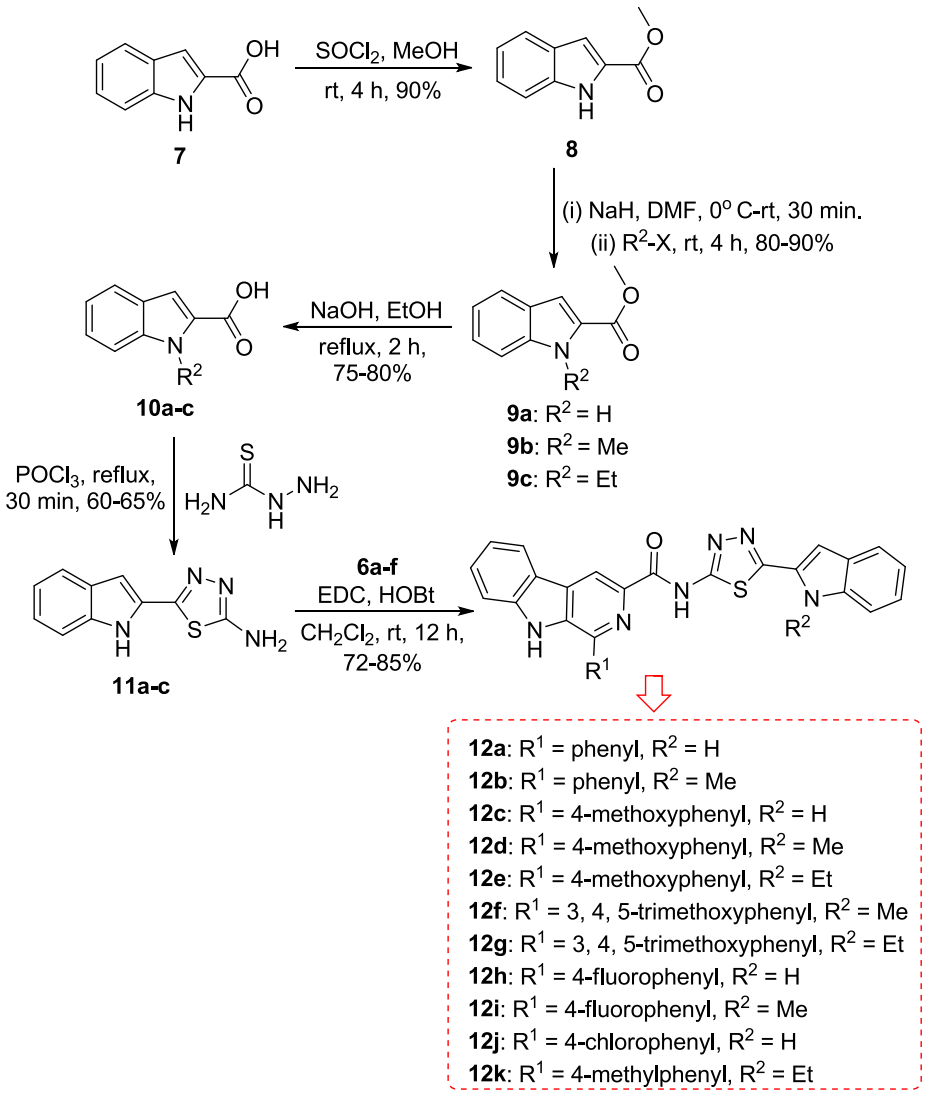

Scheme 2. Synthesis of thiadiazolo-carboxamide bridged β-carboline-indole hybrids **12a–k**.

different modes of binding of ligand result in alterations in the viscosity of DNA. The increase in viscosity is a result of an increase in the axial length of DNA to accommodate the ligand in between the base pairs, which indicates the intercalative mode of binding. However, no or minimal alteration in viscosity is observed with compounds possessing minor groove binding affinity. Conversely, covalent binders such as cisplatin result in a decrease of viscosity due to absolute functional inhibition of DNA through irreversible binding [35]. Ethidium bromide (EtBr) and Hoechst 33258 generally cause an increase and comparative alteration in relative viscosity of DNA indicating their mode of binding as intercalator and minor groove binder respectively [34].

In the current study, different concentrations of compound **12c** and **12a** along with harmine, Hoechst 33258, and EtBr are incubated with CT-DNA, and changes in viscosity were recorded. The controls EtBr and harmine displayed an increase in viscosity whereas; Hoechst 33248 exhibited a minimal change in viscosity with the increase in concentration. The tested compounds exhibited an increase in viscosity in a concentration-dependent manner indicating intercalation as their mode of DNA binding. Therefore, a graph is plotted with the concentration of compound [compound/CT-DNA] on X-axis and viscosity $[\eta/\eta_o]^{1/3}$ on Y-axis and is represented in Fig. 6.

5.2.2. Absorbance spectroscopy

Intercalation of ligands with DNA results in a slight bathochromic and significant hypochromic shift in absorbance at the specific wavelength [36]. This principle has been applied to find the efficacy of compounds **12c** and **12a** using CT-DNA.

5.2.2.1. Nanodrop method. Nanodrop is a kind of UV-spectrophotometer which uses a small quantity (nano quantity) to measure the quality of the nucleic acids [37]. The specific absorbance was measured at 260/230 nm wavelength with the different concentrations of compound **12c** and **12a** along with control CT-DNA. Harmine, Dox, Hoechst-33258, and EtBr were used as standards. It is evident from Fig. 7**A and 7B**, that compound **12c** and **12a** caused hypochromic shift at specific wavelength respectively, and are potent intercalators.

5.2.2.2. UV–Visible spectroscopy. In addition to the nanodrop method, the absorbance alterations induced by compounds **12a** and **12c** on CT-DNA were evaluated at a specific concentration along with potent intercalator EtBr as a positive control. The plain CT-DNA without the addition of any ligand was used as a control, and from Fig. 8, it is evident that the order of absorption is EtBr > **12c** > **12a**. The results of the absorbance spectroscopic methods are consistent with relative viscosity measurements and establish the intercalative mode of binding of compounds tested with CT-DNA. [38]

Table 1
Cytotoxic potential (IC_{50} values in μM) [a] of thiadiazolo-carboxamide-β-carboline-indole derivatives **12a–k** against human cell lines.

Entry	A549 [b]	MDA-MB-231 [c]	BT-474 [d]	HCT-116 [e]	HL-60 [f]	THP-1 [g]	BEAS-2B [h]
12a	3.00 ± 1.40	3.94 ± 0.31	5.68 ± 0.58	5.12 ± 1.37	8.25 ± 1.46	3.57 ± 0.55	ND
12b	9.14 ± 2.87	7.93 ± 0.33	17.55 ± 1.06	10.33 ± 1.48	33.25 ± 2.54	14.23 ± 1.25	ND
12c	2.82 ± 0.10	3.28 ± 0.43	4.09 ± 0.59	4.78 ± 1.29	3.83 ± 0.94	3.18 ± 0.49	71.25 ± 7.95
12d	8.20 ± 1.74	7.85 ± 1.77	14.08 ± 1.88	8.07 ± 0.55	30.20 ± 0.54	14.45 ± 1.17	ND
12e	14.21 ± 1.98	9.39 ± 0.52	20.13 ± 1.19	19.89 ± 1.93	46.21 ± 1.68	48.59 ± 2.11	ND
12f	7.85 ± 1.77	7.23 ± 1.43	9.15 ± 2.68	6.11 ± 2.04	10.01 ± 0.50	8.78 ± 0.27	ND
12g	10.88 ± 1.54	8.66 ± 0.30	19.47 ± 0.74	18.72 ± 2.39	43.21 ± 1.33	40.22 ± 1.21	ND
12h	3.64 ± 0.98	6.79 ± 0.57	9.20 ± 2.47	6.22 ± 0.99	9.85 ± 1.90	6.11 ± 0.43	ND
12i	9.45 ± 0.27	8.43 ± 1.30	18.36 ± 1.22	14.34 ± 2.62	37.25 ± 1.01	32.84 ± 0.97	ND
12j	3.33 ± 1.60	4.45 ± 0.91	8.68 ± 1.49	5.98 ± 0.34	9.31 ± 1.08	4.38 ± 1.28	ND
12k	9.51 ± 0.33	8.57 ± 0.40	19.53 ± 1.12	15.09 ± 3.79	39.62 ± 0.23	38.89 ± 1.57	ND
Har [i]	19.41 ± 0.66	16.74 ± 0.79	20.22 ± 0.98	25.12 ± 1.18	ND	ND	ND
Dox [j]	1.92 ± 0.86	1.48 ± 0.56	1.82 ± 0.98	ND	1.08 ± 2.02	3.25 ± 2.20	ND
VP-16 [k]	2.00 ± 1.47	ND	ND	ND	ND	ND	ND

ND: Not determined.
[a] 50% Inhibitory concentration after 72 h of drug treatment; all values are expressed as mean ± SEM, and each treatment was performed in triplicate wells.
[b] Lung cancer.
[c,d] Breast cancer.
[e] Colon cancer.
[f] Leukemia.
[g] Acute monocytic leukemia.
[h] Human bronchial lung epithelial cells. [ijk]Reference compound.
[i] Harmine.
[j] Doxorubicin.
[k] VP-16 = Etoposide

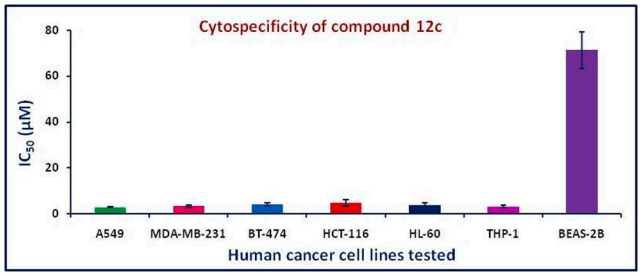

Fig. 3a. Cytospecificity exhibited by compound **12c** towards human cancer cell lines in comparison to normal human lung epithelial cells (BEAS-2B).

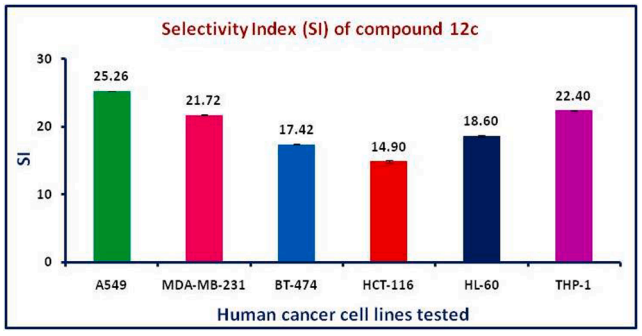

Fig. 3b. Selectivity index exhibited by compound **12c** in different human cancer cell lines.

6. Determination of apoptosis

Programmed cell death is evaded by cancer cells and prevails in the different organs; however, new cancer agents that induce apoptosis are always the prime choice of cancer research [39]. To understand the ability of compound **12c** in apoptosis induction, various qualitative (morphological) and quantitative assays were performed on the A549 lung cancer cell line.

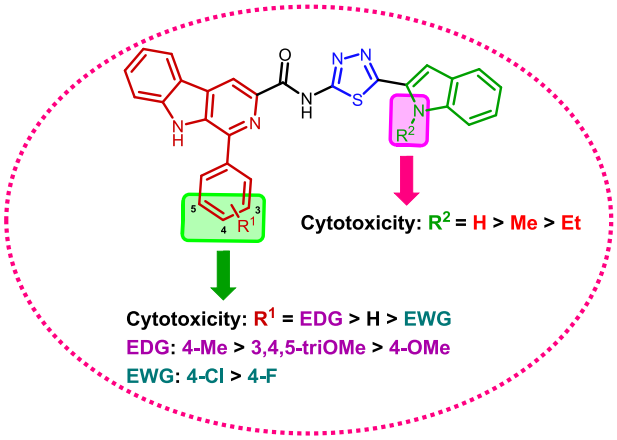

Fig. 4. Structure Activity Relationship (SAR) developed on target molecules **12a–k**.

6.1. Determination of morphological changes

The morphological assays reveal the formation of characteristic apoptotic features in the cells with the aid of different nuclear affinity dyes. Henceforth, these are the elemental line of apoptosis identification in diverse cancer cells.

6.1.1. Phase-contrast microscopy

The changes in the morphological features of A549 cells were observed after the treatment with compound **12c** at different concentrations along with the untreated control cells. Further, images reported in Fig. 9**A** were captured using phase-contrast microscopy after 72 h, reveal the characteristic apoptotic features like changes in morphology (shape, shrinkage) of the cell, reduction in the number of live cells.

6.1.2. Acridine orange staining

Acridine orange is selective toward nucleic acid and penetrates live cells and stains the nuclei green [40]. In the present study, A549 cells after treatment with compound **12c** for 72 h exhibited the formation of

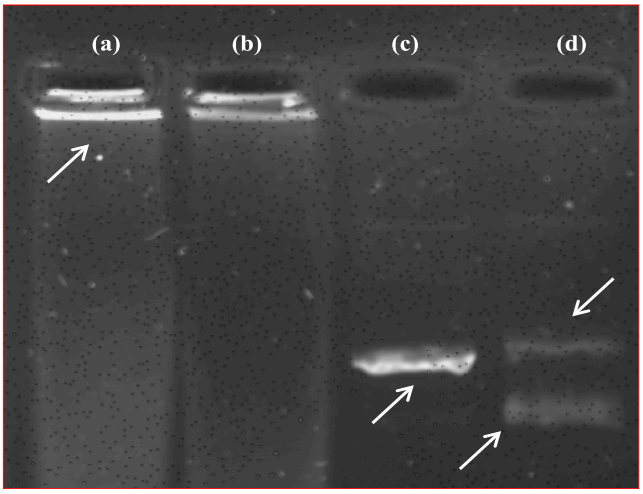

Fig. 5. Inhibition of enzyme topo IIα by compound **12c** and **12a** using horizontal gel electrophoresis. (a) Lane 1: kDNA + Topo IIα + **12c** (b) Lane 2: kDNA + Topo IIα + **12a** (c) Lane 3: DNA marker = Decatenated kDNA (d) Lane 4: DNA marker = Linear DNA. The DNA markers were obtained directly along with the kit (TG1019-1, TopoGEN, USA).

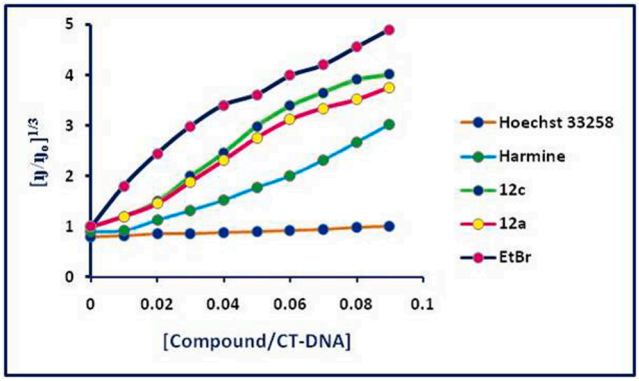

Fig. 6. Graphical representation of relative viscosity measurements of different compounds **12c** and **12a** along with different standards with CT-DNA. Hoechst33258 is negative control and EtBr: Ethidium Bromide is a positive intercalative standard.

apoptotic features such as the appearance of membrane blebs and inverse proportion in the number of cells with a concentration of compound tested. In addition, the cationic dye has the potential to bind lysosomes and thereby also exhibiting the vacuoles as represented in Fig. 9**B**.

6.1.3. DAPI staining

The initial discovery of 4,6-diamidino-2-phenylindole (DAPI) in the treatment of protozoal diseases retarded due to a strong binding affinity towards DNA base pairs. Later, this ability of passage through cell membranes made it an efficient stain to detect nuclear changes in the apoptosis cells [41]. The DAPI staining was executed according to the reported procedure [40] to detect apoptosis induction. Compound **12c** treated A549 cells after 72 h, on staining with DAPI visualized the chromatin condensation, pyknotic (inset of 1.25 μM), and condensed (bright colored: inset of 2.5 μM) nuclei formation as depicted in Fig. 9**C**.

6.2. Flow cytometry analysis

6.2.1. Quantification of apoptosis by dual staining assay

To quantify apoptotic cell death and determine the phase of apoptosis, dual staining assay with annexin V-FITC/PI was employed by using flow cytometry. The effect of different concentrations of compound **12c** on A549 cells was studied using the principle of phosphatidylserine externalization [42] and compared with control (untreated) cells. The percentage of apoptotic cells at different phases are represented on a four quadrant graph. From Fig. 10, it is clear that induction of slight early (+annexin V/– PI) and significant late apoptosis (+annexin V/+ PI) after 72 h of incubation with compound **12c**.

6.2.2. Depolarization of mitochondrial membrane potential (Δψm)

Mitochondria are the source of energy and also the crucial targets for oxidative stress in a cell [43a-b]. JC-1 staining was performed by standard protocol [43c] to assess the impact of **12c** on the mitochondrial membrane potential of A549 lung cancer cells. After the treatment period of 72 h, JC-1 dye was added and normal polarized healthy mitochondria labeled as J aggregates (red color) in the control remained intact, whereas **12c** treated resulted in the formation of depolarized mitochondria categorized as J monomers. However, the concentration of compound **12c** and the formation of J monomers increased proportionately (Fig. 11).

6.2.3. Cell cycle analysis

Cell cycle analysis was conducted on A549 cells using different concentrations (1.25, 2.5, 5 μM) of compound **12c** to figure out the phase where cells are arrested. Further, after the treatment for 48 h, cells were interpreted through the flow analyzer after staining with propidium iodide (PI). The number of cells viz., 55.68 in the G0/G1 phase in control increased exponentially to 73.27 in compound **12c** (5 μM) treated cells. It is apparent from Fig. 12**A & B** that the treatment arrested the G0/G1 phase of the cell cycle in a concentration-dependent manner.

7. Metastatic assay

Cancer cells detach from the site of origin, migrate, and develop the disease at the secondary site is known as metastasis, which makes the disease perilous and abating the survival rate of the patient [4,44].

7.1. Cell migration assay

To understand the capability of **12c** on cell migration, wound healing assay has been performed on A549 cells. This assay is based on the ability of the healing of an artificial wound called “scratch” created using a sterile pipette tip (200 μL).[45] The cells were treated with a range of concentrations varying from 1.25 to 5 μM of **12c**, along with control, and images were captured at 0 and 72 h and compared. It is inferred from Fig. 13, that the wound in control was practically healed, whereas, the cell migration is inhibited in **12c** treated cells after the period of treatment.

8. Computational analysis

8.1. Molecular docking

Further affirmation of intercalative topo-IIα inhibition by synthesized derivatives, molecular docking [46] was performed against active site of human topoisomerase II alpha complexed with DNA [47] using Glide (Schrödinger 2017–1) [48] and the best-scored compounds were detailed along with their interactive pattern. Structural accommodation of the ligand **12c** and **12a** revealed that β-carboline moiety exhibited intercalation into the DNA in the active site whereas, indole chain extended into the hydrophobic region *via* thiadiazolo carboxamide as illustrated in **A**, **C** of Fig. 14.

The analysis of docking interactions indicated that all the structural fragments (β-carboline, thiadiazole, and indole) of ligand **12c** established key interactions with residues in the active pocket such as the formation of two hydrogen bonds between amide attached thiadiazole’s nitrogen and indolic nitrogen with dC8 (d = 3.65 Å) and dT9 (d = 3.51

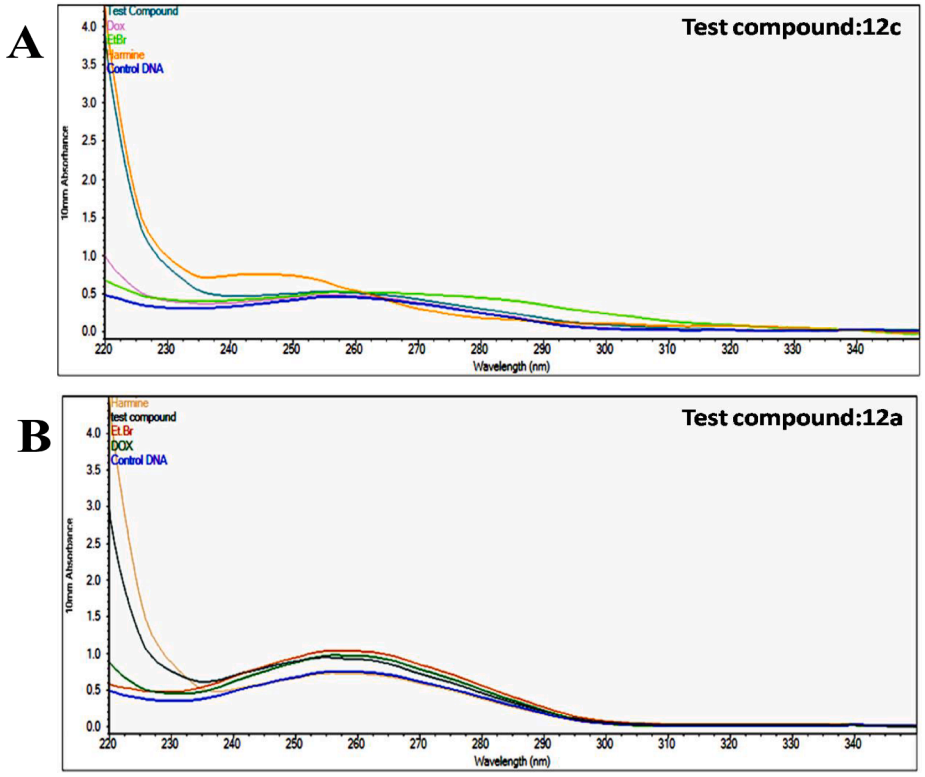

Fig. 7. Spectrophotometric analysis was performed by nanodrop spectrophotometer using CT-DNA with (**A**) Test compound: **12c** (**B**) Test compound: **12a**. EtBr and Dox were standard intercalators and control DNA is CT-DNA without any ligand. Harmine is a representative β-carboline standard.

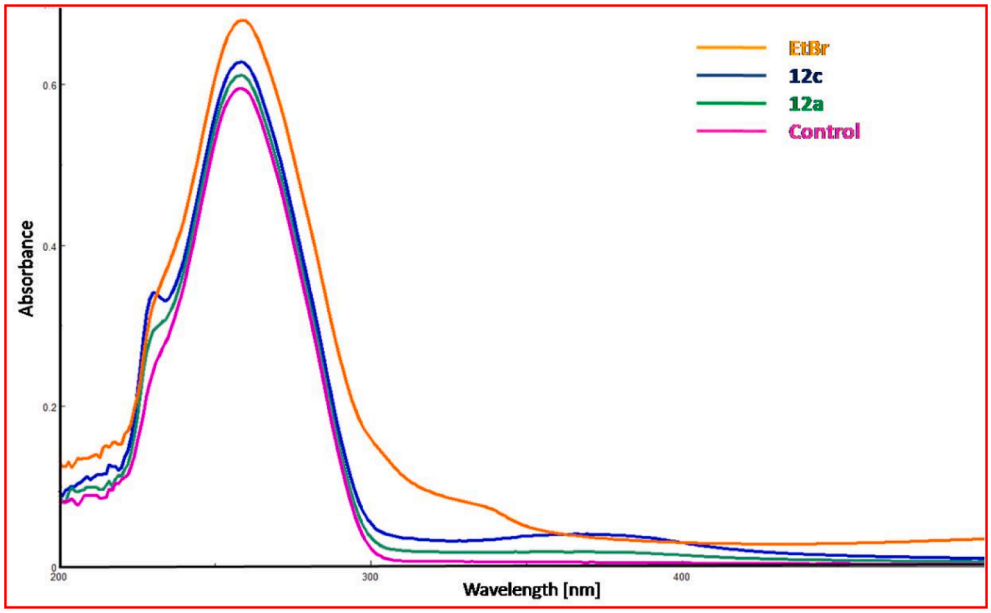

Fig. 8. Absorbance spectra of compound **12c** and **12a** with CT-DNA. EtBr is standard, whereas control is CT-DNA alone in the absence of ligand.

Å) residues respectively as represented in **B** of Fig. 14. Further, π-cation interaction was exhibited by tricyclic pyridine NH with dA12 residue and π- π interaction was observed with phenyl ring of β-carboline with dA12 and dG13 residues. Notably, several hydrophobic interactions were observed with different amino acid residues such as Leu486, Met762, Met766, Ile769, Ala801, and Pro803. Additionally, compound **12a** exhibited another crucial interaction on the β-carboline *viz* hydrogen bond between indolic N—H and Arg487 (d = 2.87 Å), along with other interactions as displayed in **D** of Fig. 14. The docking results reveal the topo II inhibition is a collective contribution by all the structural fragments (**Fig. S3, ESI)** of the compounds and are compatible with the *in vitro* biological evaluation and encourage the structural diversification on the ligands in the near future.

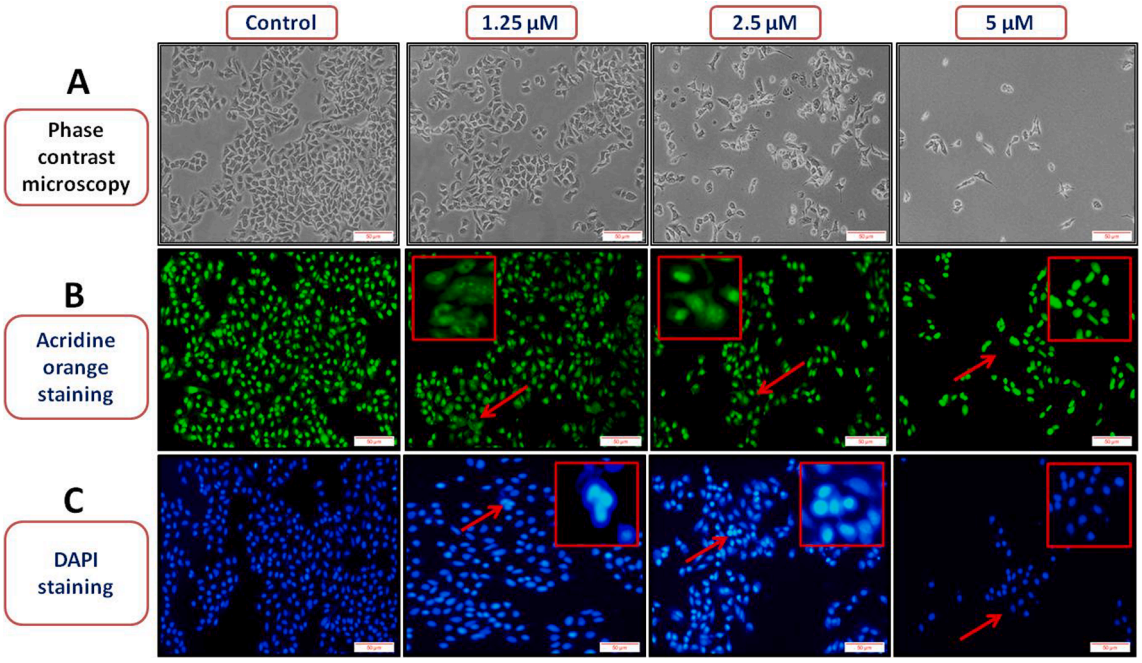

Fig. 9. Microscopic observation of the effect of different concentrations (1.25, 2.5, and 5 μM) of compound **12c** in comparison to control (untreated) on A549 cells after 72 h of treatment. The red scale bar denotes 50 μm in all the images. (**A**) Morphological changes were observed through phase-contrast microscopy. (**B**) Morphological changes such as membrane blebs were visualized through a fluorescent microscope by performing acridine orange staining. (**C**) Nuclear changes were observed by DAPI staining using a fluorescent microscope. Insets at different concentrations of treatment indicate the changes induced by treatment and red-colored arrows specify the area of effect.

8.2. *Binding energy and Lipinski's rules*

Binding energies for the molecules were calculated to identify the affinity and complex forming energy of the ligands in the active sites of the human topo-IIα complex with DNA and topo I using the prime MM/GBSA method. The lead molecules exhibited superlative binding energy values of −58.91(**12c**) and −53.67 (**12a**) kcal/mol in the active domain of 5GWK (topoisomerase IIα) in comparison to binding energy values of −46.87 (**12c**) and −40.52 (**12a**) in the active pocket of 1SC7 (topoisomerase I) (**Table S1**, **ESI**). The binding energy values of harmine and co-crystal (etoposide) are −40.94 and −72.21 kcal/mol respectively.

The drug likeliness of the potent molecules and standards (Harmine, Etoposide) was analyzed by the evaluation of the Lipinski rule of five and is incorporated in Table 2. Although the compounds other than **12a** violate the Lipinski rule in terms of molecular weight, the optimal range [49] obtained by evaluating the 95% of known drugs recommends the acceptable range up to 725 Daltons reveals the compounds tested satisfies the entire parameters and possess good drug-like properties [50,51].

8.3. *In silico ADME/T profile*

The prediction of pharmacokinetic parameters provides an idea regarding the acceptable range for human use which was obtained by analyzing 95% of known drugs [51,52]. The Physico-chemical parameters of the five best performers in the cytotoxicity table and standards (Harmine, Etoposide) were predicted by using the QikProp module [53] of Schrödinger and some key pharmacokinetic descriptors along with the recommended range are tabulated. The evaluation of computed parameters such as QPlogKhsa predicts the binding of a ligand to serum albumin which determines the availability of free drug and assessment of QPPCaco, where Caco cells act as a model for gut-blood barrier and QPPMDCK, where MDCK (Madin-Darby Canine Kidney) cells are a mimic for blood–brain barrier assist in the estimation of bioavailability. From the *in silico* data delineated in Table 3, all the newly synthesized compounds assessed through QikProp fall in the optimal range and exhibit pharmaceutical significance.

8.4. *In silico toxicity profiling*

In order to understand the toxicity profile of the synthesized compounds and harmine, TOPKAT (TOxicity Prediction by Komputer Assisted Technology) tool from Discovery Studio v19.1.0.18287 was utilized. TOPKAT employs robust and cross-validated Quantitative Structure Toxicity Relationship (QSTR) models to predict toxicological endpoints of given molecules chemical structure. Toxicity model development involves the use of 2D molecular, spatial and electronic descriptors. The optimal Predictive Space validation method of TOPKAT gives assurance to the prediction [54,55].

In silico toxicity profiling results for some of the synthesized compounds and harmine was depicted in Table 4. The toxicity profile assessment has been predicted using different animal models. The toxicity of synthesized compounds was assessed and compared with harmine in different animal models. Broadly, the probability values of the synthesized compounds showed a lower toxicity profile than harmine. All the analyzed compounds including harmine have shown higher toxicity probabilities values for Ames mutagenicity. Compounds **12a**, **12c**, **12f**, **12h** and **12j** did not show carcinogenicity call in National Toxicology Program (NTP) carcinogenicity (male and female mouse) model and found to be safe, while harmine has shown positive carcinogenicity signs in the NTP model. All the analyzed molecules had shown a positive sign for carcinogenicity in NTP (male rat) and weight of evidence rodent carcinogenicity (except **12j**) model. Except for **12f** and harmine, all the molecules had shown a negative sign for carcinogenicity in NTP (female rat) model. Moreover, all the compounds are non-degradable and negative for skin sensitization, skin irritancy and developmental toxicity potential. These compounds had shown higher probability for various animal models which include Rat Male FDA None vs Carcinogen, Rat Male FDA Single vs Multiple, Rat Female FDA None vs Carcinogen and Rat Female FDA Single vs Multiple. However, *in silico*

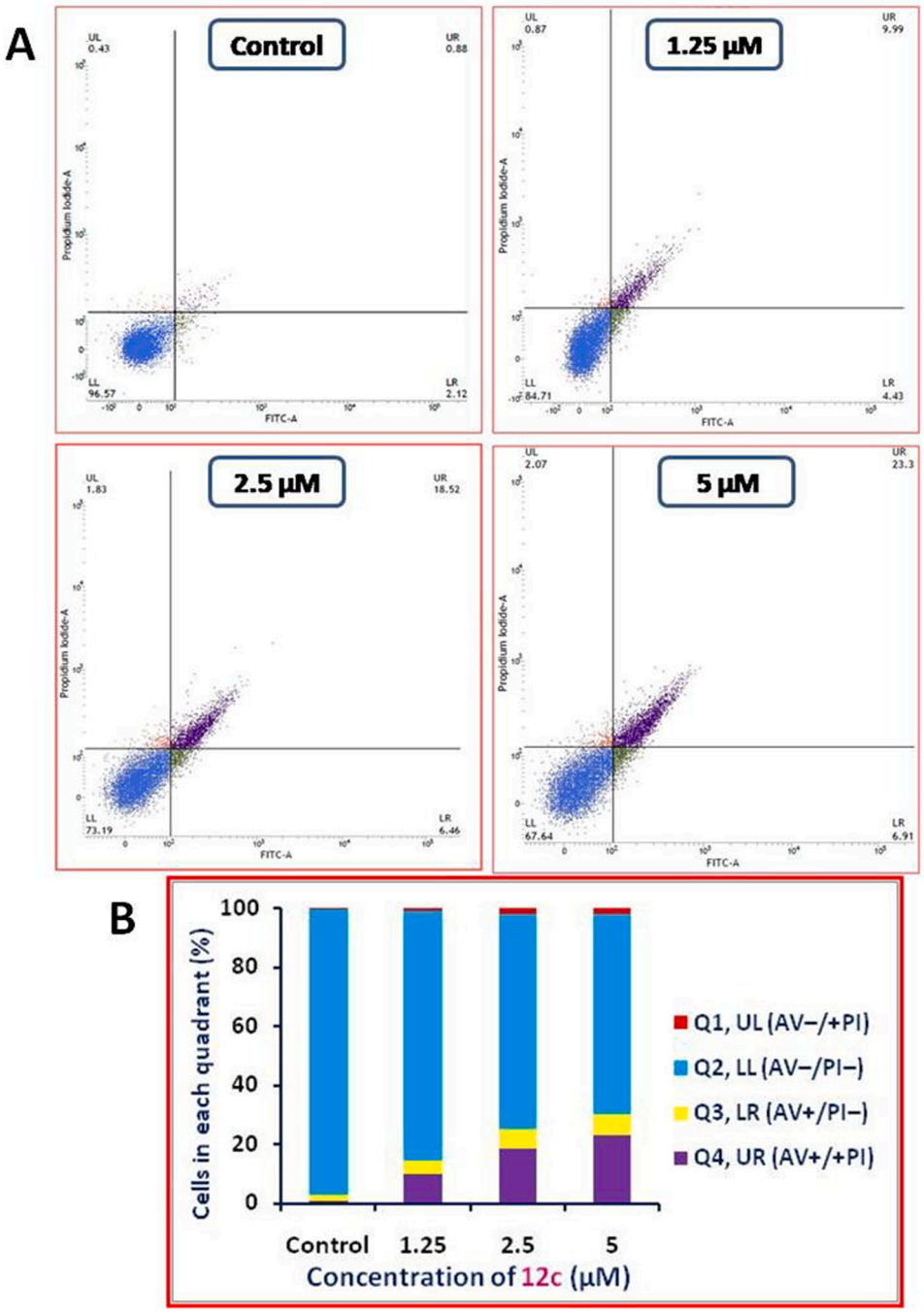

Fig. 10. Annexin V-FITC/propodium staining dual staining assay on A549 cells to determine the apoptosis induced at different concentrations (1.25, 2.5, and 5 µM) of **12c** and compared with untreated (control) cells after 72 h. (**A**) Flow cytometric analysis of each sample was analyzed and the percentage of Annexin V-FITC/PI positive cells was represented in four quadrants. (**B**) Quantification of cells in each quadrant (%) with respect to the concentration.

toxicity studies indicated that the synthesized compounds were found to be safer in many models with a minimal toxicological profile.

9. Conclusion

In summary, new molecules **12a**–**k** were rationally designed by taking into consideration of structural fragments and pharmacophoric hybridization approach to build intercalative topoisomerase IIα inhibitors targeting cancer. Based on the earlier presented pharmacophoric profile of these heterocycles (β-carboline, indolo-thiadiazole), the synthesis was performed and adjoined by carboxamide formation which resulted in the target molecules with good yields. From the preliminary *in vitro* screening, it can be observed that the compounds **12c** and **12a** remarkably expressed its cytotoxicity among all the derivatives tested in all the cell lines (solid and liquid tumors) with magnificent IC_{50} values of 2.82 ± 0.10 and 3.00 ± 1.40 µM, respectively in A549 cell line. Also, cytospecificity and selectivity index of potent compound **12c** towards cancer cells was revealed by calculating cytotoxicity (IC_{50}: 71.25 ± 7.95) against normal human lung epithelial cell line (BEAS-2B). Catalytic inhibition of topo-IIα by compounds **12c** and **12a** was evinced through gel-based electrophoresis and intercalation into DNA was revealed by evaluating alterations in parameters such as absorbance, viscosity, and correlation with standard intercalators. Additionally, deeper insights into mechanistic features by different flow cytometric

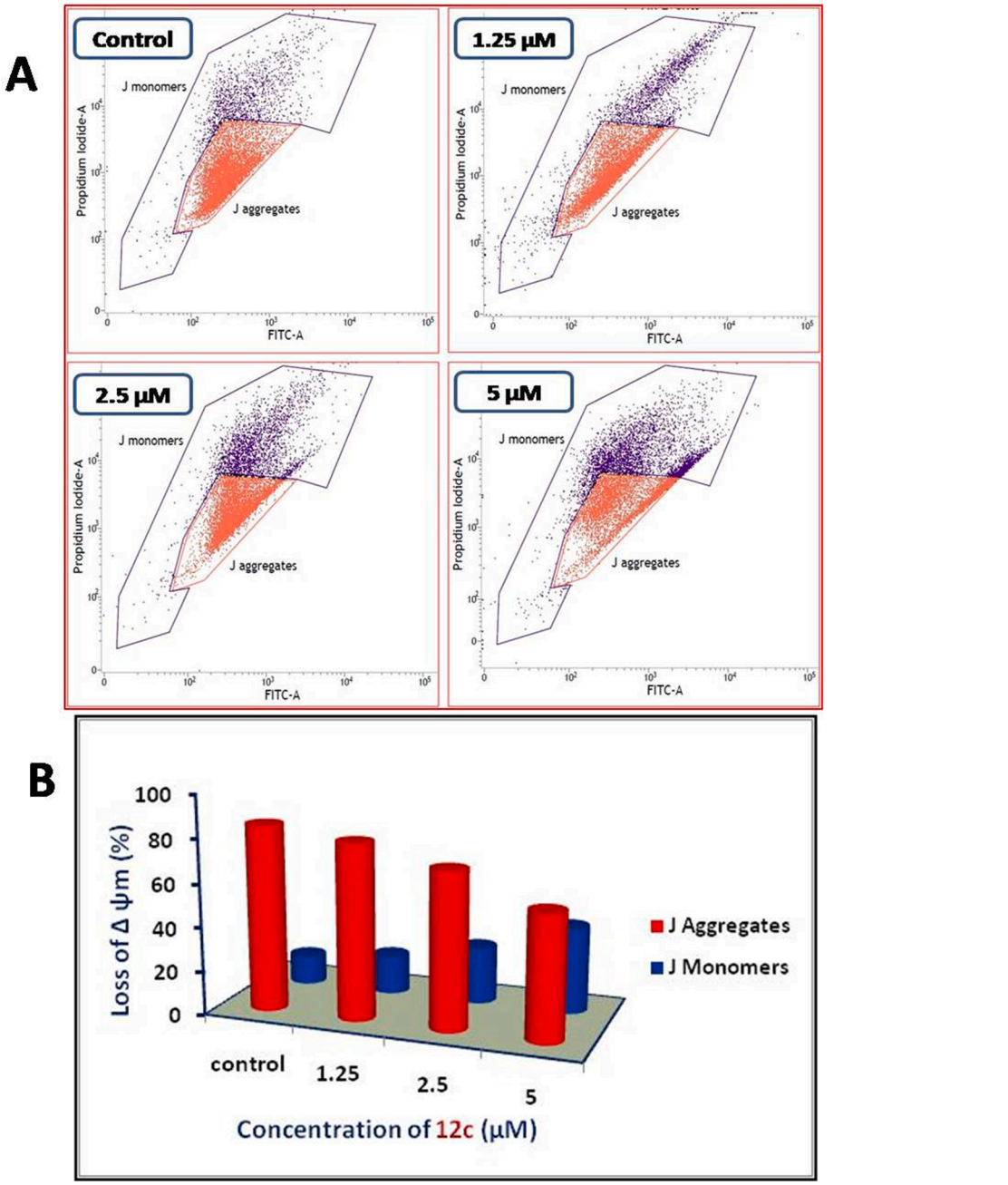

Fig. 11. Effect of different concentrations (1.25, 2.5, and 5 µM) of compound **12c** on the mitochondrial membrane potential of A549 cells after the treatment for 72 h relative to control (untreated). (**A**) Flow cytometric analysis determines the percentage of J aggregates and J monomers (**B**) Bar graph represents the quantification of J aggregates and monomers at different concentrations represented in red and blue color respectively.

assays (Annexin V/FITC, JC-1) indicated that compound **12c** is a potent inducer of apoptosis. Cell cycle progression in A549 cells was arrested at the G0/G1 phase by compound **12c** in a dose-dependent manner. Furthermore, cellular and nucleo-morphological changes caused by **12c** were also visualized using diverse staining assays (Acridine-orange and DAPI), revealed the induction of abundant apoptotic features in A549 cells. Scratch wound assay by compound **12c** indicated the inhibition of *in vitro* cell migration and deterrence of wound closure in A549 cells. Further, computational studies supported the *in vitro* target-based assays as compounds **12c** and **12a** accommodated well in the catalytic region of topo-IIα with residual amino acid and DNA base pairs interactions (PDB code: 5GWK). Further, *in silico* evaluation of ADME/T profile and drug-likeliness indicated that all the molecules fall under the specified range deduced from known drugs. As a concluding remark, the current study primarily emphasizes on assembling varied pharmacological aspects of designed compounds and can be suitably derivatized to mark their progression as promising anticancer agents.

10. Experimental section

10.1. Chemistry

Materials and methods: All the reagents and solvents were obtained from commercial suppliers and were used without further purification. Analytical thin-layer chromatography (TLC) was performed on MERCK precoated silica gel 60-F_{254} (0.5 mm) aluminium plates. Visualization of the spots on TLC plates was achieved by UV light. Wherever required, column chromatography was performed using silica gel

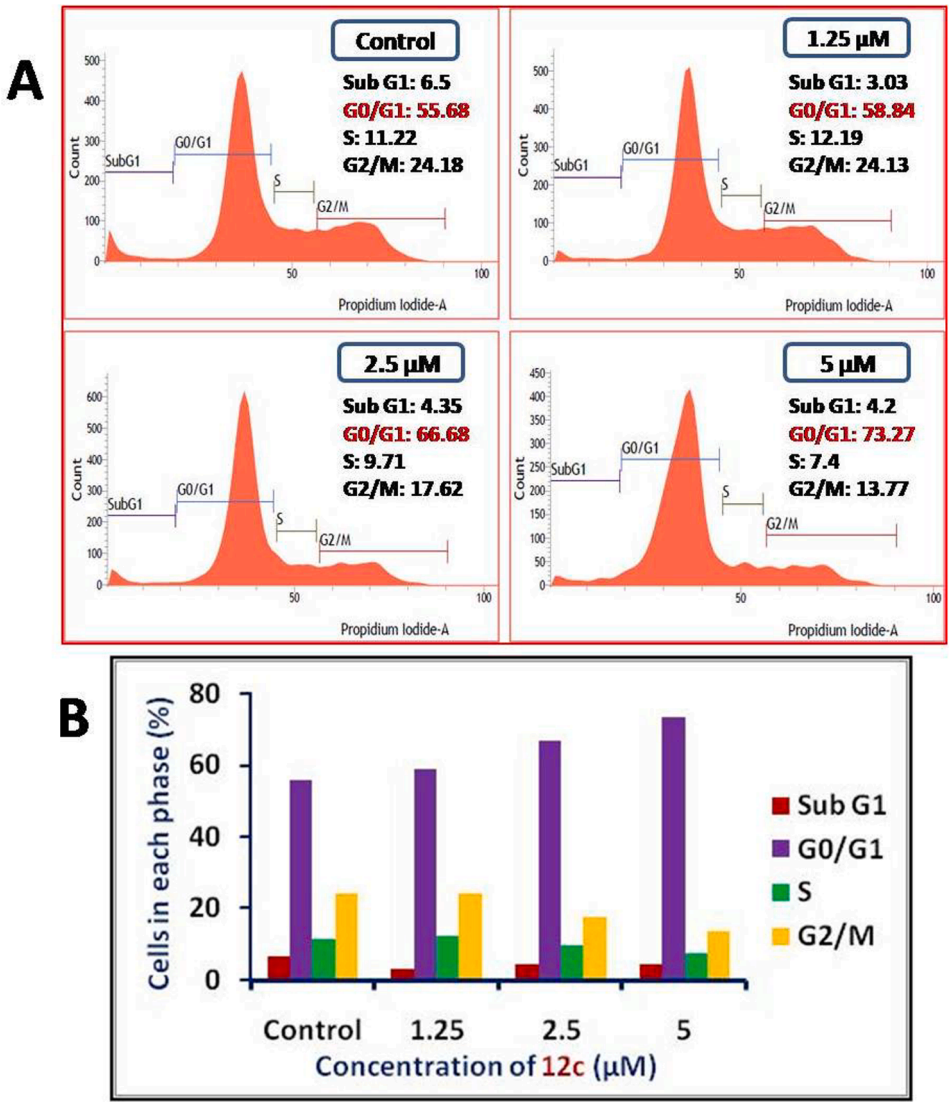

Fig. 12. Effect of varying concentrations (1.25, 2.5, and 5 µM) of potent compound **12c** on cell cycle progression in A549 cells for 48 h and compared with control (untreated). The propidium staining method was used to analyze cell cycle distribution. (**A**) Flow cytometric analysis of cell cycle distribution. (**B**) Quantification of cells at different phases of the cell cycle.

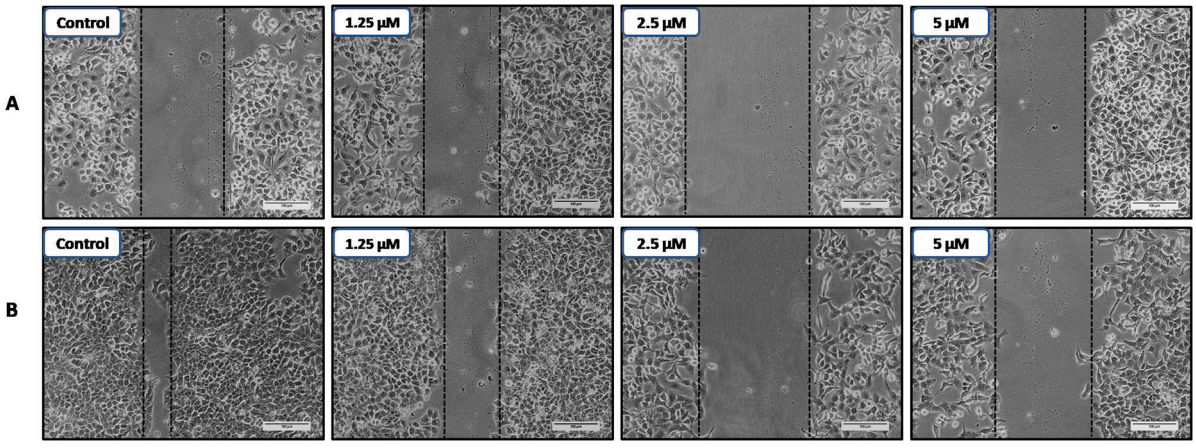

Fig. 13. Effect of compound **12c** on A549 cell migration. Cells were treated with various concentrations (1.25, 2.5, and 5 µM) of **12c**, and scratch was made using a sterile pipette tip and compared with control (untreated cells). Images were captured using a phase-contrast microscope at different periods. (**A**) Images captured at 0 h (**B**) Images captured at 72 h.

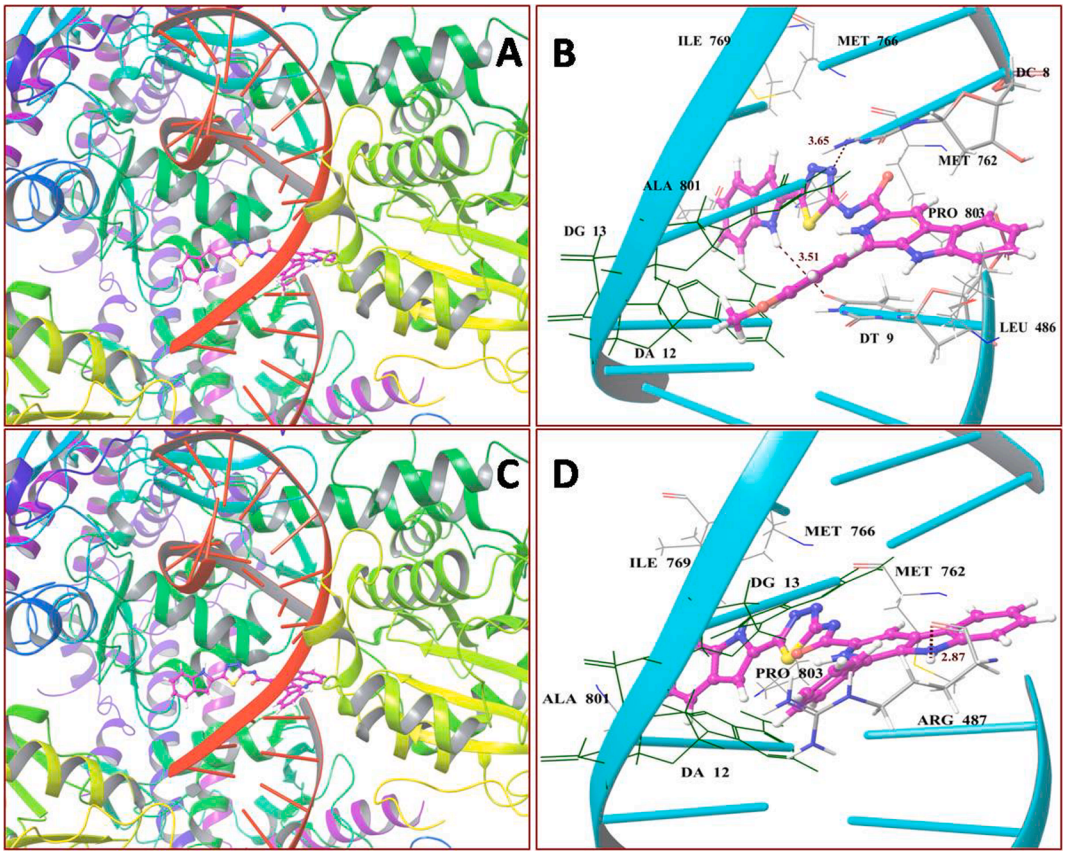

Fig. 14. Molecular docking studies. The ligands were represented in ball and stick model, carbons in ligand are colored pink and DNA in light red and cyan ribbon. (**A**) Compound **12c** in the active pocket of 5GWK. (**B**) Intercalative binding of compound **12c** along with residual interactions. (**C**) Compound **12a** in the active site of 5GWK. (**D**) Key interactions of compound **12a** with amino acids and DNA base pairs in the active site.

Table 2
Lipinski rule of five for potent hybrids and standards.

Entry	R^1	R^2	Molecular weight	H-bond donors	H-bond acceptors	QPlog P (o/w)[a]
12a	phenyl	H	486.55	3	5.5	5.63
12c	4-methoxy phenyl	H	516.58	3	6.25	5.717
12f	3,4,5-trimethoxyphenyl	Me	590.66	2	7.75	6.453
12h	4-fluorophenyl	H	504.54	3	5.5	5.863
12j	4-chlorophenyl	H	521	3	5.5	6.12
Harmine	–	–	212.25	1	1.75	3.05
VP-16[b]	–	–	588.56	3	16.95	0.60
Range or recommended values [49]			130 – 725	0 – 6.0	2 – 20	−2.0 – 6.5

[a] Predicted octanol/water partition co-efficient log P.
[b] VP-16 = Etoposide.

(60–120). The reactions wherever anhydrous conditions are required were carried under nitrogen positive pressure using freshly distilled solvents. All evaporation of solvents was carried out under reduced pressure using a rotary evaporator below 45 °C. ^{1}H and ^{13}C NMR spectra were recorded on Bruker 500 MHz by making a solution of samples in the DMSO using tetramethylsilane (TMS) as the internal standard. Chemical shifts for ^{1}H and ^{13}C are reported in parts per million (ppm) downfield from tetramethylsilane. Spin multiplicities are described as s (singlet), d (doublet), t (triplet), q (quartet), and m (multiplet). Coupling constant (*J*) values are reported in hertz (Hz). HRMS was determined with Agilent QTOF mass spectrometer 6540 series instrument. Melting points were determined with an electrothermal digital melting point apparatus IA9100 and are uncorrected. The names of all the compounds given in the experimental section were taken from Chem Bio Draw Ultra, Version 12.0.

*10.1.1. General procedure for N-(5-(1-alkyl-1H-indol-2-yl)-1,3,4-thiadiazol-2-yl)-1-aryl-9H-pyrido[3,4-b]indole-3-carboxamide (**12a–k**)*

To a mixture of 1-aryl-9*H*-pyrido[3,4-*b*]indole-3-carboxylic acid (**6a–f**, 1.1 equiv.), EDC (1.5 equiv.), HOBt (1.5 equiv.) under nitrogen conditions, dichloromethane was added and allowed to stir at room temperature for 15 min. Later, the amino component (5-(1-alkyl-indol-2-yl)-1,3,4-thiadiazol-2-amine **11a–c**, 1 equiv.) dissolved in dichloromethane, was added and the reaction was allowed to stir at room temperature till complete consumption of the starting materials as determined by TLC. The reaction mixture was extracted with dichloromethane and water (3 × 50 mL) and purified by column chromatography to yield *N*-(5-(1-alkyl-1*H*-indol-2-yl)-1,3,4-thiadiazol-2-yl)-1-phenyl-9*H*-pyrido[3,4-*b*]indole-3-carboxamide **12a–k** in moderate to good yields (72–85%).

Table 3
Physico-chemical parameters of some of the potent thiadiazolo-carboxamide bridged β-carboline-indole hybrids and standards predicted by QikProp [53]

Descriptors	Ligand entry					Standards		Recommended range
	12a	12c	12f	12h	12j	Harmine	VP-16	
EA[a] (ev)	1.24	1.25	1.25	1.28	1.27	0.48	0.22	−0.9 to 1.7
PSA[b]	101.26	106.32	108.42	101.26	101.27	33.4	166.59	70–200
SAamideO[c]	0	0	0	0	0	0	0	0–35
QPlogKhsa[d]	1.17	1.16	1.43	1.21	1.29	0.203	−0.65	−1.5 to 1.5
QPpolrz[e]	56.17	57.47	63.73	56.45	57.48	24.38	52.15	13–70
CNS[f]	−2	−2	−1	−2	−2	1	−2	−2 to +2
QPPCaco[g]	566.66	562.31	1229.128	571.09	571.56	4338.87	212.72	<25 poor, >500 great
QPlogBB[h]	−1.185	−1.146	−0.881	−1.082	−1.039	0.18	−1.59	−3 to 1.2
QPPMDCK[i]	430.3	431.40	996.531	632.96	864.13	2417.01	92.85	<25 poor, >500 great
QPlogKp[j]	−1.534	−1.483	−1.006	−1.667	−1.701	−1.34	−3.76	−8 to −1
IP[k] (ev)	8.433	8.437	8.383	8.458	8.45	8.35	8.68	7.9 to 10.5
Percent human oral absorption	94.67	83.724	95.867	83.078	84.581	100	46.24	>80% high, <25% poor

[a] PM3 calculated electron affinity.
[b] Van der Waals surface area of polar nitrogen and oxygen atoms.
[c] Solvent-accessible surface area of amide oxygen atoms.
[d] Prediction of binding to human serum albumin.
[e] Predicted polarizability in cubic angstorms.
[f] Predicted central nervous system activity.
[g] Predicted apparent Caco-2 cell permeability in nm/*sec*. Caco-2 cells are a model for the gut-blood barrier.
[h] Predicted brain/blood partition coefficient.
[i] Predicted apparent MDCK cell permeability in nm/*sec*. MDCk cells are considered to be a good mimic for the blood–brain barrier.
[j] Predicted skin permeability, log K_p.
[k] PM3 calculated ionization potential.

*10.1.1.1. N-(5-(1H-Indol-2-yl)-1,3,4-thiadiazol-2-yl)-1-phenyl-9H-pyrido[3,4-b]indole-3-carboxamide (**12a**).* Pale yellow solid; 72% yield; mp: 233–237 °C; FT-IR (cm^{-1}): 3472, 3253, 3058, 2920, 1673, 1296; ^1H NMR (500 MHz, DMSO-d_6): δ 12.58 (s, 1H), 12.19 (s, 1H), 12.14 (s, 1H), 9.13 (s, 1H), 8.55 (d, $J = 7.9$ Hz, 1H), 8.39 (d, $J = 7.1$ Hz, 2H), 7.84–7.62 (m, 6H), 7.52 (d, $J = 8.1$ Hz, 1H), 7.44 (t, $J = 7.4$ Hz, 1H), 7.27 (t, $J = 7.1$ Hz, 1H), 7.22 (d, $J = 1.4$ Hz, 1H), 7.13 (t, $J = 7.4$ Hz, 1H).; ^{13}C NMR (125 MHz, DMSO-d_6): δ 164.1, 158.2, 156.0, 142.1, 142.1, 137.9, 137.5, 137.3, 135.5, 130.3, 129.7, 129.5, 129.4, 129.2, 128.4, 128.2, 123.9, 122.6, 121.6, 121.4, 121.1, 120.4, 115.6, 113.3, 112.4, 104.5; HRMS (ESI): *m/z* calcd for $C_{28}H_{18}N_6OS$ 487.1336 found 487.1334 $[M+H]^+$.

*10.1.1.2. N-(5-(1-Methyl-1H-indol-2-yl)-1,3,4-thiadiazol-2-yl)-1-phenyl-9H-pyrido[3,4-b]indole-3-carboxamide (**12b**).* Pale yellow solid; 75% yield; mp: 287–291 °C; FT-IR (cm^{-1}): 3622, 3207, 1686, 1592, 1407, 1244; ^1H NMR (500 MHz, DMSO-d_6): δ 12.56 (s, 1H), 12.10 (s, 1H), 9.08 (s, 1H), 8.50 (d, $J = 7.9$ Hz, 1H), 8.33 (d, $J = 7.1$ Hz, 2H), 7.76–7.59 (m, 7H), 7.38 (t, $J = 7.6$ Hz, 1H), 7.32 (t, $J = 7.6$ Hz, 1H), 7.19 (s, 1H), 7.15 (t, $J = 7.3$ Hz, 1H), 4.18 (s, 3H); ^{13}C NMR (125 MHz, DMSO-d_6): δ 164.2, 158.3, 156.3, 142.1, 139.4, 137.5, 137.2, 135.5, 130.3, 129.7, 129.5, 129.4, 129.2, 129.0, 127.3, 124.1, 122.6, 121.6, 121.5, 121.1, 120.8, 115.6, 113.3, 111.0, 106.6, 32.6; HRMS (ESI): *m/z* calcd for $C_{29}H_{20}N_6OS$ 501.1492 found 501.1489 $[M+H]^+$.

*10.1.1.3. N-(5-(1H-Indol-2-yl)-1,3,4-thiadiazol-2-yl)-1-(4-methoxyphenyl)-9H-pyrido[3,4-b]indole-3-carboxamide (**12c**).* Pale yellow solid; 73% yield; mp: 265–270 °C; FT-IR (cm^{-1}): 3430, 3528, 3054, 1691, 1025, 893; ^1H NMR (500 MHz, DMSO-d_6): δ 12.50 (s, 1H), 12.15 (s, 1H), 12.04 (s, 1H), 9.02 (s, 1H), 8.48 (d, $J = 7.9$ Hz, 1H), 8.31 (d, $J = 8.7$ Hz, 2H), 7.75 (d, $J = 8.2$ Hz, 1H), 7.69–7.60 (m, 2H), 7.47 (d, $J = 8.2$ Hz, 1H), 7.37 (t, $J = 7.1$ Hz, 1H), 7.23 (dd, $J = 17.3$, 8.0 Hz, 3H), 7.17 (d, $J = 1.4$ Hz, 1H), 7.08 (t, $J = 7.1$ Hz, 1H), 3.93 (s, 3H); ^{13}C NMR (125 MHz, DMSO-d_6): δ 164.2, 160.6, 158.2, 156.0, 142.1, 142.0, 137.9, 137.1, 135.3, 131.0, 130.1, 130.0, 129.3, 128.4, 128.2, 123.9, 122.6, 121.6, 121.4, 121.0, 120.4, 115.0, 114.6, 113.3, 112.4, 104.5, 55.8; HRMS (ESI): *m/z* calcd for $C_{29}H_{20}N_6O_2S$ 517.1441 found 517.1436 $[M+H]^+$.

*10.1.1.4. 1-(4-Methoxyphenyl)-N-(5-(1-methyl-1H-indol-2-yl)-1,3,4-thiadiazol-2-yl)-9H-pyrido[3,4-b]indole-3-carboxamide (**12d**).* Pale yellow solid; 72% yield; mp: 287–291 °C; FT-IR (cm^{-1}): 3277, 3055, 1671, 1407, 1042, 1026; ^1H NMR (500 MHz, DMSO-d_6): δ 12.46 (s, 1H), 12.02 (s, 1H), 9.00 (s, 1H), 8.45 (d, $J = 7.9$ Hz, 1H), 8.37–8.13 (m, 2H), 7.73 (d, $J = 8.2$ Hz, 1H), 7.67 (d, $J = 7.9$ Hz, 1H), 7.62 (t, $J = 8.1$ Hz, 1H), 7.59 (d, $J = 8.1$ Hz, 1H), 7.36 (t, $J = 7.2$ Hz, 1H), 7.31 (t, $J = 7.6$ Hz, 1H), 7.24 (d, $J = 8.8$ Hz, 2H), 7.20–7.03 (m, 2H), 4.17 (s, 3H), 3.93 (s, 3H); ^{13}C NMR (125 MHz, DMSO-d_6): δ 164.2, 160.7, 158.3, 156.2, 142.1, 139.4, 137.1, 135.3, 130.9, 130.1, 130.0, 129.3, 129.0, 127.3, 124.1, 122.5, 121.6, 121.5, 121.0, 120.8, 115.1, 114.7, 113.3, 110.9, 106.6, 55.9, 32.6; HRMS (ESI): *m/z* calcd for $C_{30}H_{22}N_6O_2S$ 531.1598 found 531.1595 $[M+H]^+$.

*10.1.1.5. N-(5-(1-Ethyl-1H-indol-2-yl)-1,3,4-thiadiazol-2-yl)-1-(4-methoxyphenyl)-9H-pyrido[3,4-b]indole-3-carboxamide (**12e**).* Pale yellow solid; 74% yield; mp: 278–282 °C; FT-IR (cm^{-1}): 3370, 3283, 2974, 1674, 1495,1031; ^1H NMR (500 MHz, DMSO-d_6): δ 12.48 (s, 1H), 12.05 (s, 1H), 9.03 (s, 1H), 8.47 (d, $J = 7.9$ Hz, 1H), 8.29 (d, $J = 8.8$ Hz, 2H), 7.75 (d, $J = 8.2$ Hz, 1H), 7.68 (d, $J = 7.9$ Hz, 1H), 7.66–7.58 (m, 2H), 7.37 (t, $J = 7.1$ Hz, 1H), 7.32 (t, $J = 7.1$ Hz, 1H), 7.26 (d, $J = 8.8$ Hz, 2H), 7.19 (d, $J = 0.5$ Hz, 1H), 7.15 (t, $J = 7.1$ Hz, 1H), 4.77 (q, $J = 7.0$ Hz, 2H), 3.93 (s, 3H), 1.36 (t, $J = 7.1$ Hz, 3H); ^{13}C NMR (125 MHz, DMSO-d_6): δ 164.2, 160.6, 158.2, 156.1, 142.0, 138.3, 137.0, 135.3, 130.9, 130.0, 129.9, 129.3, 128.1, 127.5, 124.1, 122.6, 121.7, 121.6, 121.0, 120.8, 115.1, 114.6, 113.3, 110.9, 107.0, 55.9, 27.3, 15.8; HRMS (ESI): *m/z* calcd for $C_{31}H_{24}N_6O_2S$ 545.1754 found 545.1747 $[M+H]^+$.

*10.1.1.6. N-(5-(1-Methyl-1H-indol-2-yl)-1,3,4-thiadiazol-2-yl)-1-(3,4,5-trimethoxyphenyl)-9H-pyrido[3,4-b]indole-3-carboxamide (**12f**).* Pale yellow solid; 85% yield; mp: 225–230 °C; FT-IR (cm^{-1}): 2942, 1736, 1683, 1001, 905, 782; ^1H NMR (500 MHz, DMSO-d_6): δ 12.50 (s, 1H), 12.09 (s, 1H), 9.07 (s, 1H), 8.50 (d, $J = 7.9$ Hz, 1H), 7.73 (d, $J = 8.2$ Hz, 1H), 7.69 – 7.66 (m, 1H), 7.65–7.54(m, 2H), 7.47–7.42 (m, 2H), 7.38 (t, $J = 6.5$ Hz, 1H), 7.33 (t, $J = 10.5$ Hz, 1H), 7.20 (s, 1H), 7.15 (t, $J = 7.1$ Hz, 1H), 4.19 (s, 3H), 4.00 (s, 6H), 3.83 (s, 3H); ^{13}C NMR (125 MHz, DMSO-d_6): δ 164.3, 158.2, 156.3, 153.6, 142.4, 142.07, 139.4, 138.9, 137.0, 135.6, 132.9, 130.0, 129.4, 129.0, 127.3, 124.1, 122.7, 121.6, 121.5, 121.0, 120.8, 115.6, 113.3, 111.0, 107.1, 106.6, 60.5, 56.6, 32.6;

Table 4
Probability values of different toxicity models for lead compounds and harmine by TOPKAT analysis.

TOPKAT MODEL	12a	12c	12f	12h	12j	Harmine
Aerobic_Biodegradability	−12.1 (Non-Degradable)	−10.9 (Non-Degradable)	−8.81 (Non-Degradable)	−13.5 (Non-Degradable)	−20.6 (Non-Degradable)	−4.31 (Non-Degradable)
Ames_Mutagenicity	8.02 (Mutagen)	6.11 (Mutagen)	5.98 (Mutagen)	5.99 (Mutagen)	5.7 (Mutagen)	7.15 (Mutagen)
Developmental_Toxicity_Potential	−3.72 (Non-Toxic)	−0.859 (Non-Toxic)	−1.13 (Non-Toxic)	−1.35 (Non-Toxic)	−2.51 (Non-Toxic)	−0.421 (Non-Toxic)
Mouse_Female_FDA_None_vs_Carcinogen	−0.797 (Carcinogen)	−4.72 (Non-Carcinogen)	−5.39 (Non-Carcinogen)	−1.46 (Non-Carcinogen)	−3.87 (Non-Carcinogen)	1.83 (Carcinogen)
Mouse_Female_FDA_Single_vs_Multiple	−4.48 (Single-Carcinogen)	–	–	–	–	0.879 (Multiple-Carcinogen)
Mouse_Female_NTP	−0.856 (Non-Carcinogen)	−3.07 (Non-Carcinogen)	0.818 (Non-Carcinogen)	−1.43 (Non-Carcinogen)	−2.11 (Non-Carcinogen)	2.58 (Carcinogen)
Mouse_Male_FDA_None_vs_Carcinogen	1.49 (Carcinogen)	−0.662 (Carcinogen)	−2.13 (Non-Carcinogen)	−1.72 (Carcinogen)	−2.31 (Non-Carcinogen)	2.8 (Carcinogen)
Mouse_Male_FDA_Single_vs_Multiple	−10.8 (Single-Carcinogen)	−10 (Single-Carcinogen)	–	−13.7 (Single-Carcinogen)	–	−4.03 (Multiple-Carcinogen)
Mouse_Male_NTP	−5.02 (Non-Carcinogen)	−5.35 (Non-Carcinogen)	−4.97 (Non-Carcinogen)	−5.26 (Non-Carcinogen)	−3.75 (Non-Carcinogen)	1.84 (Carcinogen)
Ocular_Irritancy_Mild_vs_Moderate_Severe	−3.2 (Mild)	−4.54 (Mild)	−4.62 (Mild)	−2.61 (Mild)	−2.61 (Mild)	1.22 (Moderate_Severe)
Rat_Female_FDA_None_vs_Carcinogen	−1.2 (Carcinogen)	3.25 (Carcinogen)	3.49 (Carcinogen)	−0.979 (Carcinogen)	−2.83 (Non-Carcinogen)	4.66 (Carcinogen)
Rat_Female_FDA_Single_vs_Multiple	−0.0137 (Single-Carcinogen)	1.12 (Multiple-Carcinogen)	−1.49 (Single-Carcinogen)	1.99 (Multiple-Carcinogen)	–	−0.139 (Single-Carcinogen)
Rat_Female_NTP	−1.36 (Non-Carcinogen)	0.0595 (Non-Carcinogen)	2.93 (Carcinogen)	−2.7 (Non-Carcinogen)	−2.7 (Non-Carcinogen)	1.48 (Carcinogen)
Rat_Male_FDA_None_vs_Carcinogen	3.45 (Carcinogen)	4.55 (Carcinogen)	7.61 (Carcinogen)	5.36 (Carcinogen)	3.06 (Carcinogen)	4.21 (Carcinogen)
Rat_Male_FDA_Single_vs_Multiple	−5.08 (Single-Carcinogen)	−4.07 (Single-Carcinogen)	−4.74 (Single-Carcinogen)	−5.85 (Single-Carcinogen)	−6.54 (Single-Carcinogen)	−1.15 (Single-Carcinogen)
Rat_Male_NTP	3.21 (Carcinogen)	2.1 (Carcinogen)	7.24 (Carcinogen)	3.3 (Carcinogen)	1.25 (Carcinogen)	0.968 (Carcinogen)
Skin_Irritancy_None_vs_Irritant	−1.82 (Non-Irritant)	−1.9 (Non-Irritant)	−1.56 (Non-Irritant)	−2.28 (Non-Irritant)	−2.28 (Non-Irritant)	−4.66 (Mild)
Skin_Sensitization_None_vs_Sensitizer	−4.14 (Non-Sensitizer)	−3.54 (Non-Sensitizer)	−5.06 (Non-Sensitizer)	−3.53 (Non-Sensitizer)	−3.53 (Non-Sensitizer)	−2.95 (Non-Sensitizer)
Weight_of_Evidence_Rodent_Carcinogenicity	1.46 (Carcinogen)	0.889 (Carcinogen)	1.21 (Carcinogen)	2.05 (Carcinogen)	−0.0222 (Non-Carcinogen)	1.08 (Carcinogen)
Carcinogenic_Potency_TD50_Mouse	0.506 mg/kg	0.622 mg/kg	1.08 mg/kg	0.477 mg/kg	0.364 mg/kg	32 mg/kg
Carcinogenic_Potency_TD50_Rat	0.228 mg/kg	0.0373 mg/kg	0.0266 mg/kg	0.0649 mg/kg	0.0601 mg/kg	3.01 mg/kg
Chronic_LOAEL	0.036 g/kg	0.0211 g/kg	0.0177 g/kg	0.0288 g/kg	0.0264 g/kg	0.0139 g/kg
Daphnia_EC50	0.0539 mg/l	0.0257 mg/l	0.0382 mg/l	0.053 mg/l	0.0375 mg/l	1.6 mg/l
Fathead_Minnow_LC50	2.07e-05 g/l	9.2e-06 g/l	2.19e-06 g/l	2.21e-05 g/l	1.12e-05 g/l	0.0392 g/l
Rat_Inhalational_LC50	7.65e + 03 mg/m3/h	1.03e + 04 mg/m3/h	6.33e + 03 mg/m3/h	1.25e + 04 mg/m3/h	5.14e + 03 mg/m3/h	2.43e + 04 mg/m3/h
Rat_Maximum_Tolerated_Dose_Feed	0.165 g/kg	0.0771 g/kg	0.039 g/kg	0.216 g/kg	0.199 g/kg	0.0441 g/kg
Rat_Maximum_Tolerated_Dose_Gavage	0.00422 g/kg	0.000328 g/kg	4.86e-05 g/kg	0.000435 g/kg	0.000336 g/kg	0.00477 g/kg
Rat_Oral_LD50	2.89 g/kg	2.69 g/kg	1.88 g/kg	1.75 g/kg	3.37 g/kg	0.202 g/kg

HRMS (ESI): *m/z* calcd for $C_{32}H_{26}N_6O_4S$ 591.1809 found 591.1805 $[M+H]^+$.

*10.1.1.7. N-(5-(1-Ethyl-1H-indol-2-yl)-1,3,4-thiadiazol-2-yl)-1-(3,4,5-trimethoxyphenyl)-9H-pyrido[3,4-b]indole-3-carboxamide (**12g**).* Pale yellow solid; 78% yield; mp: 283–286 °C; FT-IR (cm^{-1}): 3280, 2971, 1706, 1507, 1353, 1246; ^{1}H NMR (500 MHz, DMSO-d_6): δ 12.46 (s, 1H), 12.10 (s, 1H), 9.08 (s, 1H), 8.50 (d, J = 7.9 Hz, 1H), 7.73 (d, J = 8.2 Hz, 1H), 7.70–7.56 (m, 3H), 7.47 (s, 2H), 7.38 (t, J = 7.2 Hz, 1H), 7.32 (t, J = 7.2 Hz, 1H), 7.20 (s, 1H), 7.15 (t, J = 7.4 Hz, 1H), 4.77 (dd, J = 14.0, 6.9 Hz, 2H), 4.00 (s, 6H), 3.83 (s, 3H), 1.36 (t, J = 7.1 Hz, 3H); ^{13}C NMR (125 MHz, DMSO-d_6): δ 164.1, 158.2, 156.2, 153.6, 142.4, 142.0, 138.9, 138.3, 136.9, 135.5, 132.9, 130.0, 129.4, 128.0, 127.5, 124.2, 122.6, 121.7, 121.6, 121.1, 120.8, 115.5, 113.3, 110.8, 107.0, 106.9, 60.6, 56.5, 15.7; HRMS (ESI): *m/z* calcd for $C_{33}H_{28}N_6O_4S$ 605.1996 found 605.1991 $[M+H]^+$.

*10.1.1.8. N-(5-(1H-Indol-2-yl)-1,3,4-thiadiazol-2-yl)-1-(4-fluorophenyl)-9H-pyrido[3,4-b]indole-3-carboxamide (**12h**).* Pale yellow solid; 76% yield; mp: 260–265 °C; FT-IR (cm^{-1}): 3463, 3335, 1456, 1042, 892, 861; ^{1}H NMR (500 MHz, DMSO-d_6): δ 12.64 (s, 1H), 12.16 (s, 1H), 12.11 (s, 1H), 9.08 (s, 1H), 8.50 (d, J = 7.9 Hz, 1H), 8.45–8.41 (m, 2H), 7.75 (d, J = 8.2 Hz, 1H), 7.68–7.63 (m, 2H), 7.53 (t, J = 8.9 Hz, 2H), 7.47 (d, J = 8.2 Hz, 1H), 7.39 (t, J = 7.4 Hz, 1H), 7.22 (t, J = 7.1 Hz, 1H), 7.17 (d, J = 1.4 Hz, 1H), 7.08 (t, J = 7.1 Hz, 1H); ^{13}C NMR (125 MHz, DMSO-d_6): δ 164.2, 162.3, 158.3, 156.0, 142.1, 141.1, 137.9, 137.3, 135.4, 133.9, 131.9 (d, J = 8.4 Hz), 130.4, 129.4, 128.4, 128.2, 123.9, 122.6, 121.6, 121.4, 121.1, 120.4, 116.2, 116.1, 115.9, 115.6, 113.3, 112.4, 104.5; HRMS (ESI): *m/z* calcd for $C_{28}H_{17}FN_6OS$ 505.1241 found 505.1236 $[M+H]^+$.

*10.1.1.9. 1-(4-Fluorophenyl)-N-(5-(1-methyl-1H-indol-2-yl)-1,3,4-thiadiazol-2-yl)-9H-pyrido[3,4-b]indole-3-carboxamide (**12i**).* Pale yellow solid; 73% yield; mp: 270–275 °C; FT-IR (cm^{-1}): 3299, 3064, 1673, 1605, 1408, 843; ^{1}H NMR (500 MHz, DMSO-d_6): δ 12.64 (s, 1H), 12.10 (s, 1H), 9.07 (s, 1H), 8.49 (d, J = 7.9 Hz, 1H), 8.46–8.32 (m, 2H), 7.74 (d, J = 8.2 Hz, 1H), 7.66 (dd, J = 15.3, 7.5 Hz, 2H), 7.60 (d, J = 8.1 Hz, 1H), 7.53 (t, J = 8.9 Hz, 2H), 7.38 (t, J = 7.4 Hz, 1H), 7.32 (t, J = 7.1 Hz, 1H), 7.19 (s, 1H), 7.15 (t, J = 7.1 Hz, 1H), 4.19 (s, 3H); ^{13}C NMR (125 MHz, DMSO-d_6): δ 164.3, 158.3, 156.3, 142.1, 141.1, 139.4, 137.2, 135.4, 134.0, 131.9, 131.9, 130.4, 129.4, 129.0, 127.3, 124.1, 121.6, 121.5, 121.1, 120.8, 116.1, 116.0, 115.7, 113.3, 111.0, 106.6, 32.6; HRMS (ESI): *m/z* calcd for $C_{29}H_{19}FN_6OS$ 519.1398 found 519.1397 $[M+H]^+$.

*10.1.1.10. N-(5-(1H-Indol-2-yl)-1,3,4-thiadiazol-2-yl)-1-(4-chlorophenyl)-9H-pyrido[3,4-b]indole-3-carboxamide (**12j**).* Pale yellow solid; 82% yield; mp: 285–290 °C; FT-IR (cm^{-1}): 3293, 2919, 2855, 1624, 1093, 1013; ^{1}H NMR (500 MHz, DMSO-d_6): δ 12.65 (s, 1H), 12.14 (d, J = 17.3 Hz, 2H), 9.09 (s, 1H), 8.50 (d, J = 7.9 Hz, 1H), 8.41 (t, J = 7.6 Hz, 2H), 8.12 (d, J = 8.5 Hz, 1H), 7.77–7.73 (m, 2H), 7.70 (d, J = 8.5 Hz, 1H), 7.64 (d, J = 7.7 Hz, 1H), 7.47 (d, J = 8.2 Hz, 1H), 7.39 (t, J = 7.5 Hz, 1H), 7.22 (t, J = 7.3 Hz, 1H), 7.15 (t, J = 10.9 Hz, 1H), 7.08 (t, J = 7.4 Hz, 1H); ^{13}C NMR (125 MHz, DMSO-d_6): δ 164.2, 158.3, 156.0, 142.2, 140.7, 137.9, 137.4, 136.7, 136.3, 135.5, 134.5, 131.5, 131.0, 130.5, 129.5, 129.3, 129.1, 128.4, 128.2, 123.9, 122.7, 121.6, 121.4, 121.1, 120.4, 113.3, 112.4, 104.5; HRMS (ESI): *m/z* calcd for $C_{28}H_{17}ClN_6OS$ 521.0946 found 521.0939 $[M+H]^+$.

*10.1.1.11. N-(5-(1-Ethyl-1H-indol-2-yl)-1,3,4-thiadiazol-2-yl)-1-(p-tolyl)-9H-pyrido[3,4-b]indole-3-carboxamide (**12k**).* Pale yellow solid; 76% yield; mp: 228–232 °C; FT-IR (cm^{-1}): 3283, 3068, 1739, 1625, 1245,823; ^{1}H NMR (500 MHz, DMSO-d_6): δ 12.45 (s, 1H), 12.04 (s, 1H), 9.05 (s, 1H), 8.48 (d, J = 7.9 Hz, 1H), 8.21 (d, J = 8.0 Hz, 2H), 7.74 (d, J = 8.2 Hz, 1H), 7.68 (d, J = 7.9 Hz, 1H), 7.66–7.57 (m, 2H), 7.52 (d, J = 7.9 Hz, 2H), 7.38 (t, J = 7.5 Hz, 1H), 7.32 (t, J = 7.6 Hz, 1H), 7.19 (s, 1H), 7.15 (t, J = 7.5 Hz, 1H), 4.77 (q, J = 7.0 Hz, 2H), 2.50 (s, 3H), 1.36 (t, J = 7.1 Hz, 3H); ^{13}C NMR (125 MHz, DMSO-d_6): δ 164.2, 158.2, 156.1, 142.2, 142.1, 139.3, 138.4, 137.1, 135.5, 134.7, 130.2, 129.8, 129.4, 128.1, 127.5, 124.1, 122.6, 121.7, 121.0, 120.8, 115.4, 113.3, 110.9, 107.0, 21.4, 15.8; HRMS (ESI): *m/z* calcd for $C_{31}H_{24}N_6OS$ 529.1805 found 529.1800 $[M+H]^+$.

10.2. Biological evaluation

10.2.1. Cell culture

Normal human bronchial epithelial cell line (BEAS-2B) and cancer cell lines like lung (A549), breast (MDA-MB-231, BT-474), colon (HCT-116), Leukemia (HL-60, THP-1), were maintained in appropriate media supplemented with 10% fetal bovine serum (FBS) stabilized with 1% antibiotic–antimycotic solution (Sigma Aldrich) and cells were maintained at 37 °C with 5% CO_2 and 98% relative humidity in the incubator. When the cells reached up to 80–90% of confluency, sub-culturing was performed using a 0.25% trypsin/1 mM EDTA solution for further passage. The stock solution of 10 mM was prepared by dissolving test compounds and standards in DMSO. Required concentrations were further obtained by suitable dilutions with respective media.

10.2.2. MTT assay

MTT (3-(4,5-dimethylthiazol-2-yl)-2,5-diphenyl tetrazolium bromide) is a dye that converts into insoluble formazan by mitochondrial succinate dehydrogenase enzyme, where MTT assay is a colorimetric assay, thereby measures the reduction of MTT. Metabolically active cells can reduce the MTT and the level of activity indicates the viability of cells. Briefly, cells were seeded in 96-well plates at a density of 1000 to 4000 cells per well in 100 μL of complete medium and allowed to grow overnight for attachment onto the wells. After the media was replaced with fresh media, the cells were treated with various concentrations of the compounds for a period of 72 h. After incubation, the media was aspirated and 100 μL of MTT (0.5 mg/mL) was added and incubated at 37 °C for 4 h. Then MTT reagent was aspirated and the formazan crystals formed were dissolved by the addition of 200 μL of DMSO for 20 min. at 37 °C. The formazan product quantity was measured by using a spectrophotometric microtiter plate reader (Spectra Max, M4 Molecular Devices, USA) at 570 nm wavelength.

10.3. Target-based assays

10.3.1. Topoisomerase IIα inhibition

Topo IIα inhibition of potent compounds **12c** and **12a** at a concentration of 10 μM was evaluated by performing ATP dependent decatenation of kDNA by the protocol described in the Drug Screening Kit of Topo II (TG1019-1, TopoGEN, USA). Reactions were carried out in 20 μL and contained two different types of buffer in equal ratio and 200–300 ng of kDNA, and topoisomerase II (TG2000H-2, TopoGEN, USA). The quantity of topoisomerase II (5 units) was attuned in pilot experiments to decatenate around 100% of the kDNA under our assay conditions. Authentic decatenated DNA and linear DNA was used as a control to identify the changes. The samples were made with buffer, kDNA, test compounds, topo-IIα and incubated at 37 °C for 30 min. and terminated by the addition of 2 μL of a stop buffer containing 10% (w/v) SDS and 2 μL of 0.5 mg/mL proteinase-K and incubated for 10 min at 37 °C. After completion of the reaction, the products in the reaction mixture were separated by 1% agarose gel. The products in the agarose gel were visualized after staining with ethidium bromide (0.2 mg/mL). The gels were run at 100 V for about 30 min. and visualized under UV transillumination (BIO-RAD gel doc XR+, USA).

10.3.2. DNA intercalation assays

10.3.2.1. Relative viscosity studies. The viscosities of the DNA-ligand complexes were determined by the Lovis 2000 M/ME Rolling-ball viscometer (Anton Paar GmbH, Graz, Austria), based on the falling ball principle. The temperature was controlled at ±0.005 K through an internal Peltier thermostat. A calibrated 1.59 mm glass capillary containing a steel ball was filled with the sample for measuring the ball falling time at angles in the range from 20° to 70°. The kinematic, as well as dynamic viscosities at 25 °C, were estimated based on the ball falling time and densities DNA solution was prepared in 100 mM Tris-HCl (pH 7.4) and viscosity was measured while each derivative **12c** and **12a** (5 μM) was added to CT-DNA solution (50 μM). Ethidium bromide, Harmine and Hoechst 33258 at different concentrations were used as controls. Data was represented graphically as $(\eta/\eta_0)^{1/3}$ vs. the ratio of the concentration of the hybrid to CT-DNA, where η is the viscosity of CT-DNA in the presence of the various concentrations of derivatives and η_0 is the viscosity of CT-DNA solution.

10.3.2.2. Absorbance spectroscopy

10.3.2.2.1. DNA nanodrop method. DNA intercalation is determined by nanodrop spectrophotometric analysis. The intercalating agents decrease the absorption and increase the wavelengths. In our experiment, we incubated the 50 μM of calf thymus DNA (Sigma-Aldrich, USA) with compound **12c** and **12a**, Ethidium bromide (EtBr), Doxorubicin (DOX) and Harmine for 10 min at 1 μM concentration. Later, the TAE buffer used as blank and absorbance and concentrations were determined by NanoDrop™ 2000/2000c Spectrophotometer (Thermo Fisher Scientific, USA).

10.3.2.2.2. UV–Visible spectroscopy. DNA intercalation is determined by UV–Visible spectroscopic analysis. In our experiment, we incubated the 50 μM of calf thymus DNA (Sigma-Aldrich, USA) with compound **12c** and **12a**, and Ethidium bromide (EtBr), for 10 min at 1 μM concentration and compared with control (i.e. CT-DNA alone). Later, the TAE buffer used as blank and absorbance and concentrations were determined by UV–Visible Spectrophotometer (Jasco; V-650).

10.4. Apoptosis detection studies

10.4.1. Morphological observations

10.4.1.1. Phase-contrast microscopy. A549 cells were plated in 12 well culture plates with a cell density of 1×10^6 cells/mL and allowed to adhere overnight. The cells were incubated with different (1.25, 2.5, and 5 μM) concentrations of the compound **12c** for 72 h treatment. Later cells were checked for the morphological changes, and images were taken using a phase-contrast microscope (Nikon, Inc. Japan).

10.4.1.2. Acridine orange (AO) staining. A549 cells were plated at a concentration of 1×10^6 cells/mL and treated with various concentrations of compound **12c** and the plates were incubated for 72 h. 10 μL of fluorescent dye, Acridine Orange (AO) was added into each well in equal volumes (10 μg/ml) respectively then the cells were visualized immediately under a fluorescence microscope (Nikon, Inc. Japan) with excitation (488 nm) and emission (550 nm) at 200X magnification.

10.4.1.3. DAPI nucleic acid staining. DAPI staining aids in the observation of morphological changes in the nucleus. After treatment with compound **12c** for 72 h, lung cancer A549 cells were washed with PBS and permeabilized with 0.1% Triton X for 10 min followed by staining with 1 μM DAPI. Control and treated cells were observed with a fluorescence microscope with excitation at 359 nm and emission at 461 nm using DAPI filter at 200X magnification.

10.4.2. Flow cytometric analysis

10.4.2.1. Annexin V assay. This assay was performed by the method [56] given by Rieger *et al.* with slight modifications. Briefly, 1×10^5 cells were seeded in a 12-well plate and treated with different concentrations of compound **12c** for 72 h. The collected cells were washed twice with ice-cold PBS, then incubated with 200 μL of 1× binding buffer containing 1 μL propidium iodide (PI) for 15 min. at room temperature in the dark. After incubation, cells were analyzed for apoptosis using a flow cytometer (BD FACSVerseTM, USA). Apoptosis and necrosis were analyzed with quadrant statistics on propidium iodide-negative cells, fluorescein positive cells, and propidium iodide (PI)-positive cells, respectively.

10.4.2.2. Measurement of mitochondrial membrane potential. A549 cells (1×10^6 cells/ml) were seeded in 12 well plates and allowed to adhere overnight. The cells were incubated with compound **12c** at 1.25, 2.5, and 5 μM concentrations for 72 h. Cells were collected and washed with PBS and resuspended in a solution of JC-1 (1 μM) and incubated for 30 min. in an incubator at 37 °C. The cells were washed twice with PBS and analyzed by flow cytometer (BD FACSVerse™, USA).

10.4.2.3. Cell cycle analysis. In general, the novel compounds exert their cytotoxic or growth inhibitory effect by arresting the specific checkpoint in the cell cycle. Flow cytometric analysis (FACS) was performed to calculate the distribution of the cell population in various cell cycle phases. Here A549 cancer cells were incubated with compound **12c** at various concentrations from 1.25 to 5 μM for 48 h. Untreated and treated cells were harvested, washed, and fixed overnight in 70% ethanol in PBS at −20 °C. Fixed cells were pelleted and stained with cell cycle analysis reagent propidium iodide (50 μg/ml) with RNase A for 20 min at 37 °C in dark according to the manual instructions and about 10,000 events were acquired and analyzed on a flow cytometer BD FACSVerse™ (BD Biosciences, USA).

10.5. Metastatic assays

10.5.1. Cell migration assay/wound healing assay

A549 cells were plated at a cell density of 3.5×10^5 cells/well into 12-well plates in RPMI medium and allowed to form a confluent monolayer, and then the scratch is made with 200 μL sterile pipette tip and then treated with 1.25, 2.5 and 5 μM of the compound **12c**. The migration of lung cancer cells were captured by microscopic observations at 0 h and 72 h.

10.6. Computational studies

The DNA crystal structure has been retrieved from Protein Data Bank (PDB ID: 5GWK) [46] and 1SC7. The protein preparation tool was used for the preparation of the human topoisomerase II alpha with DNA and topoisomerase I. The missing atoms will be added up and peripheral water molecules will be removed with a distance of less than 5 Å from the pocket through the protein preparation wizard. The grid is generated by picking the active site where the co-crystal is located with a grid box of 10 × 10 × 10 Å (Schrödinger 2017–1) [47]. The potent hybrids were sketched (**12c** & **a**) by using 2D sketcher and energy minimized, and prepared using Ligprep for the generation of different conformers (Schrödinger 2017–1). The different conformers thus obtained were subjected to molecular docking with SP Glide (Schrödinger 2017–1). The poses generated were evaluated and the best one was described. Five potent compounds and standards were subjected to ligand preparation and the diverse conformers thus generated were envisaged for their Physico-chemical parameters using QikProp [52]. The different descriptors were thus reported.

Declaration of Competing Interest

The authors declare that they have no known competing financial interests or personal relationships that could have appeared to influence the work reported in this paper.

Acknowledgments

Authors are thankful to DoP, Ministry of Chemicals & Fertilizers, Govt. of India, New Delhi, for the award of the NIPER fellowship. We acknowledge Dr. Chandraiah Godugu and his lab members, Department of Regulatory Toxicology, NIPER, Hyderabad for all time support to carry out the biological studies. NIPER-H Research Communication No.: NIPER-H/2020/M035.

Appendix A. Supplementary material

Supplementary data to this article can be found online at https://doi.org/10.1016/j.bioorg.2020.104357.

References

[1] World Health Organization, Cancer Fact Sheet https://www.who.int/news-room/fact-sheets/detail/cancer/ (accessed March 31, 2020).
[2] (a) WHO. WHO Virtual press conference on COVID-19. https://www.who.int/docs/default-source/coronaviruse/transcripts/who-audio-emergencies-coronavirus-press-conference-full-and-inal11mar2020.pdf?sfvrsn=cb432bb3_2 (accessed on 31 March 2020). (b) J. Bedford, D. Enria, J Giesecke, D. L Heymann, C. Ihekweazu, G. Kobinger, H C. Lane, Z. Memish, M-d. Oh, A. A. Sall, A. Schuchat, K. Ungchusak, L. H. Wieler, COVID-19: towards controlling of a pandemic, The Lancet, (2020) https://doi.org/10.1016/S0140-6736(20)30673-5. (c) K.S. Saini, C. Lanza, M. Romano, E. de Azambuja, J. Cortes, B. de las Heras, J. de Castro, M.L. Saini, S. Loibl, G. Curigilano, C. Twelves, M. Leone, M.M. Patnaik, Repurposing anticancer drugs for COVID-19-induced inflammation, immune dysfunction, and coagulopathy, Br. J. Cancer, 123 (2020) 694–697.
[3] L.A. Loeb, K.R. Loeb, J.P. Anderson, Multiple mutations and cancer, PNAS 100 (2003) 776–781.
[4] (a) T.N. Seyfried, L.C. Huysentruyt, On the origin of cancer metastasis. Crit. Rev. Oncol. 18 (2013) 43–73. (b) https://www.cancer.net/navigating-cancer-care/cancer-basics/what-metastasis (accessed March 31, 2020).
[5] (a) W.T. Beck, Multidrug resistance and its circumvention, Eur. J. Cancer 26 (1990) 513–515. (b) S. Nekkanti, O. Ommi, P.S.S. Lakshmi, N. Shankaraiah, Diverse targeted approaches to battle multidrug resistance in cancer, 26 (2019) 7059–7080. (c) A. Kamal, S. Nekkanti, N. Shankaraiah, S. Manda (Eds.), Future of Drug Discovery: Drug Resistance in Bacteria, Fungi, Malaria, and Cancer, Springer International Publishing, (2017) 609–629.
[6] (a) US National Cancer Institute, Cancer Statistics, https://www.cancer.gov/about-cancer/understanding/statistics (accessed March 31, 2020). (b) R.L. Siegel, K.D. Miller, A. Jemal, Cancer statistics, CA: A Cancer J. Clin. (2020) https://doi.org/10.3322/caac.21590.
[7] http://www.exploredna.co.uk/the-importance-dna.html.
[8] F. Pi, Z. Zhao, V. Chelikani, K. Yoder, M. Kvaratskhelia, P. Guo, Development of potent antiviral drugs inspired by viral hexameric DNA-packaging motors with revolving mechanism, J. Virol. 90 (2016) 8036–8046.
[9] (a) J. Yan, K. Wang, W. Dang, R. Chen, J. Xie, B. Zhang, J. Song, R. Wang, Two hits are better than one: membrane-active and DNA binding-related double-action mechanism of NK-18, a novel antimicrobial peptide derived from mammalian NK-lysin, Antimicrob Agents Chemother. 57 (2013) 220–228;

(b) T.J. Opperman, S.M. Kwasny, J. Bo Li, M.A. Lewis, D. Aiello, J.D. Williams, N. P. Peet, D.T. Moir, T.L. Bowlin, E.C. Long, DNA targeting as a likely mechanism underlying the antibacterial activity of synthetic bis-indole antibiotics, Antimicrob Agents Chemother. 60 (2016) 7067–7076;
(c) N.B. Dyatkina, C.D. Roberts, J.D. Keicher, Y. Dai, J.P. Nadherny, W. Zhang, U. Schmitz, A. Kongpachith, K. Fung, A.A. Novikov, L. Lou, M. Velligan, A. A. Khorlin, M.S. Chen, Minor groove DNA binders as microbial agents. 1. Pyrrole tetramides are potent antibacterials against vancomycin resistant *Enterococci* and methicillin resistant *Staphylococcus aureus*, J. Med. Chem. 45 (2002) 805–817.

[10] X. Li, Y. Lin, Q. Wang, Y. Yuan, H. Zhang, X. Qian, The novel anti-tumor agents of 4-triazol-1,8-naphthalimides: synthesis, cytotoxicity, DNA intercalation and photocleavage, Eur. J. Med. Chem. 46 (2011) 1274–1279.

[11] (a) M.F. Branea, M. Cacho, A. Gradillas, B. Pascual-Teresa, A. Ramos, Intercalators as anticancer drugs, Curr. Pharm. Des 7 (2001) 1745–e1780;
(b) Z. Chen, R. Cao, B. Shi, L. Guo, J. Sun, Q. Ma, W. Fan, H. Song, Synthesis and biological evaluation of 1,3-disubstituted β-carbolines as potent DNA intercalating and cytotoxic agents, Eur. J. Med. Chem. 46 (2011) 5127–5137;
(c) S. Nekkanti, R. Tokala, N. Shankaraiah, Targeting DNA minor groove by hybrid molecules as anticancer agents, Curr. Med. Chem. 24 (2017) 2887–2907.

[12] M. Sathish, B. Kavitha, V.L. Nayak, Y. Tangella, A. Ajitha, S. Nekkanti, A. Alarifi, N. Shankaraiah, N. Nagesh, A. Kamal, Synthesis of podophyllotoxin linked β–carboline congeners as potential anticancer agents and DNA topoisomerase II inhibitors, Eur. J. Med. Chem. 144 (2018) 557–571.

[13] (a) A. Sakaguchi, A. Kikuchi, Functional compatibility between isoform α and β of type II DNA topoisomerase, J. Cell. Sci. 117 (2004) 1047–1054;
(b) T.J. Wendorff, B.H. Schmidt, P. Heslop, C.A. Austin, J.M. Berger, The structure of DNA-bound human topoisomerase II alpha: conformational mechanisms for coordinating inter-subunit interactions with DNA cleavage, J. Mol. Biol. 424 (2012) 109–124;
(c) C.A. Austin, K.L. Marsh, Eukaryotic DNA topoisomerase II beta, Bioessays 20 (1998) 215–226;
(d) F.H. Drake, G.A. Hofmann, H.F. Bartus, M.R. Mattern, S.T. Crooke, C. K. Mirabelli, Biochemical and pharmacological properties of p170 and p180 forms of topoisomerase II, Biochemistry 28 (1989) 8154–8160;
(e) F.H. Drake, J.P. Zimmerman, F.L. McCabe, H.F. Bartus, S.R. Per, D.M. Sullivan, W.E. Ross, M.R. Mattern, R.K. Johnson, S.T. Crooke, C.K. Mirabelli, Purification of topoisomerase II from amsacrine-resistant P388 leukemia cells. Evidence for two forms of the enzyme, J. Biol. Chem. 262 (1987) 16739–16747;
(f) J.R. Jenkins, P. Ayton, T. Jones, S.L. Davies, D.L. Simmons, A.L. Harris, D. Sheer, I.D. Hickson, Isolation of cDNA clones encoding the b isozyme of human DNA topoisomerase II and localisation of the gene to chromosome 3p24, Nucleic Acids Res. 20 (1992) 5587–5592.

[14] (a) W. Hu, X. Huang, J. Wu, L. Yang, Y. Zheng, Y. Shen, Z. Li, X. Li, Discovery of novel topoisomerase II inhibitors by medicinal chemistry approaches, J. Med. Chem. 61 (2018) 8947–8980;
(b) J. Wesierska-Gadek, A. Skladanowski, Therapeutic intervention by the simultaneous inhibition of DNA repair and type I or type II DNA topoisomerases: one strategy, many outcomes, Future Med. Chem. 4 (2012) 51–72;
(c) R. Karki, C. Park, K. Jun, J. Lee, P. Thapa, T.M. Kadayat, Y. Kwon, E. Lee, Synthesis, antitumor activity, and structure-activity relationship study of trihydroxylated 2,4,6-triphenyl pyridines as potent and selective topoisomerase II inhibitors, Eur. J. Med. Chem. 84 (2014) 555–565.

[15] D. Hanahan, R.A. Weinberg, Hallmarks of cancer: the next generation, Cell 5 (2011) 646–674.

[16] M.K. Ibrahim, M.S. Taghour, A.M. Metwaly, A. Belal, A.B.M. Mehany, M. A. Elhendawy, M.M. Radwan, A.M. Yassin, N.M. El-Deeb, E.E. Hafez, M.A. Elsohly, I.H. Eissa, Design, synthesis, molecular modeling and anti-proliferative evaluation of novel quinoxaline derivatives as potential DNA intercalators and topoisomerase II inhibitors, Eur. J. Med. Chem. 155 (2018) 117–134.

[17] R. Tokala, S. Thatikonda, U.S. Vanteddu, S. Sana, C. Godugu, N. Shankaraiah, Design and synthesis of DNA-interactive β-carboline-oxindole hybrids as cytotoxic and apoptosis inducing agents, ChemMedChem 13 (2018) 1909–1922.

[18] (a) M.M. Gonzalez, M. Pellon-Maison, M.A. Ales-Gandolfo, M.R. Gonzalez-Baro, R. Erra-Balsells, F.M. Cabrerizo, Photosensitized cleavage of plasmidic DNA by norharmane, a naturally occurring beta-carboline, Org. Biomol. Chem. 8 (2010) 2543–2552;
(b) J. Kovvuri, B. Nagaraju, V.L. Nayak, R. Akunuri, M.P.N. Rao, A. Ajitha, N. Nagesh, A. Kamal, Design, synthesis and biological evaluation of new β-carboline-bisindole compounds as DNA binding, photocleavage agents and topoisomerase I inhibitors, Eur J Med Chem. 143 (2018) 1563–1577;
(c) H. Guan, X. Liu, W. Peng, R. Cao, Y. Ma, H. Chen, A. Xu, Beta-carboline derivatives: novel photosensitizers that intercalate into DNA to cause direct DNA damage in photodynamic therapy, Biochem. Bioph. Res. Co. 342 (2006) 894–901.

[19] (a) A. Kamal, M. Sathish, V.L. Nayak, V. Srinivasulu, B. Kavitha, Y. Tangella, D. Thummuri, C. Bagul, N. Shankaraiah, N. Nagesh, Design and synthesis of dithiocarbamate linked β-carboline derivatives: DNA topoisomerase II inhibition with DNA binding and apoptosis inducing ability, Bioorg. Med. Chem. 23 (2015) 5511–5526;
(b) A.M. Deveau, M.A. Labroli, C.M. Dieckhuas, M.T. Barthen, K.S. Smith, T. L. Macdonald, The synthesis of amino-acid functionalized beta-carbolines as topoisomerase II inhibitors, Bioorg. Med. Chem. Lett. 11 (2001) 1251–1255.

[20] (a) K. Huber, L. Brault, O. Fedorov, C. Gasser, P. Filippakopoulos, A.N. Bullock, D. Faabbro, J. Trappe, J. Schwaller, S. Knapp, F. Bracher, 7,8-Dichloro-1-oxo- β-carbolines as a versatile scaffold for the development of potent and selective kinase inhibitors with unusual binding modes, J. Med. Chem. 55 (2012) 403–413;
(b) Y. Song, J. Wang, S.F. Teng, D. Kesuma, Y. Deng, J. Duan, J.H. Wang, R.Z. Qi, M.M. Sim, β-carbolines as specific inhibitors of cyclin-dependent kinases, Bioorg. Med. Chem. Lett. 12 (2002) 1129–1132;
(c) G.D. Cuny, N.P. Ulyanova, D. Patnaik, J.F. Liu, X. Lin, K. Auerbach, S.S. Ray, J. Xian, M.A. Glicksman, R.L. Stein, J.M. Higgins, Structure-activity relationship study of beta-carboline derivatives as haspin kinase inhibitors, Bioorg. Med. Chem. Lett. 22 (2012) 2015–2019;
(d) J. Zhang, Y. Li, L. Guo, R. Cao, P. Zhao, W. Jiang, Q. Ma, H. Yi, Z. Li, J. Jiang, J. Wu, Y. Wang, S. Si, DH166, a beta-carboline derivative, inhibits the kinase activity of PLK1, Cancer Biol. Ther. 24 (2009) 2374–2383.

[21] (a) R. Cao, W. Peng, Z. Wang, A. Xu, Beta-carboline alkaloids: biochemical and pharmacological functions, Curr. Med. Chem. 14 (2007) 479–500;
(b) Z. Li, S. Chen, S. Zhu, J. Luo, Y. Zhang, Q. Weng, Synthesis and fungicidal activity of β-carboline alkaloids and their derivatives, Molecules 20 (2015) 13941–13957;
(c) P. Ashok, S. Ganguly, S. Murugesan, Review on in-vitro antimalarial activity of natural β-carboline alkaloids, Mini Rev. Med. Chem. 13 (2013) 1778–1791.

[22] A. Abdildinova, Y. Gong, Current parallel solid-phase synthesis of drug-like oxadiazole & thiadiazole derivatives for combinatorial chemistry, ACS Comb. Sci. 20 (2018) 309–329.

[23] S.I. Farooqi, N. Arshad, P.A. Channar, F. Perveen, A. Saeed, F.A. Larik, A. Javeed, Synthesis, theoretical, spectroscopic and electrochemical DNA binding investigations of 1, 3, 4-thiadiazole derivatives of ibuprofen and ciprofloxacin: Cancer cell line studies, J. Photochem. Photobio. B. 189 (2018) 104–118.

[24] T. Plech, B. Kapron, A. Paneth, M. Wujec, R. Czamomysy, A. Bielawska, K. Bielawski, N. Trotsko, E. Kusmierz, P. Paneth, Search for human DNA topoisomerase II poisons in the group of 2,5-disubstituted-1,3,4-thiadiazoles, J. Enzyme Inhib. Med. Chem. 30 (2015) 1021–1026.

[25] (a) Y. Wan, Y. Li, C. Yan, M. Yan, Z. Tang, Indole: A privileged scaffold for the design of anti-cancer agents, Eur. J. Med. Chem. 183 (2019) 111691–111711;
(b) S. Dadashpour, S. Emami, Indole in the target-based design of anticancer agents: A versatile scaffold with diverse mechanisms, Eur. J. Med. Chem. 150 (2018) 9–29;
(c) P.V. Thanikachalam, R.K. Maurya, V. Garg, V. Monga, An insight into the medicinal perspective of synthetic analogs of indole: A review, Eur. J. Med. Chem. 180 (2019) 562–612;
(d) K. Kaur, V. Jaitak, Recent development in indole derivatives as anticancer agents for breast cancer, Anticancer Agents Med Chem. 19 (2018) 962–983;
(e) A. Kumari, R.K. Singh, Medicinal chemistry of indole derivatives: current to future therapeutic prospective, Bioorg. Chem. 89 (2019), 103021.

[26] N.K. Kaushik, N. Kaushik, P. Attri, N. Kumar, C.H. Kim, A.K. Verma, E.H. Choi, Biomedical importance of indoles, Molecules 18 (2013) 6620–6662.

[27] N. Shankaraiah, A.P. Sakla, K. Laxmikeshav, R. Tokala, Reliability of click chemistry on drug discovery, Chem. Rec. 19 (2019) 1–21.

[28] (a) C. Lazar, A. Kluczyk, T. Kiyota, Y. Konishi, Drug evolution concept in drug design: 1. Hybridization method, J Med. Chem. 47 (2004) 6973–6982;
(b) J.A. Ortega, L. Riccardi, E. Minniti, M. Borgogno, J.M. Arencibia, M.L. Greco, A. Minarini, C. Sissi, M.D. Vivo, Pharmacophore hybridization to discover novel topoisomerase II poisons with promising antiproliferative activity, J. Med. Chem. 61 (2018) 1375–1379.

[29] (a) R. Tokala, S. Thatikonda, S. Sana, P. Regur, C. Godugu, N. Shankaraiah, Synthesis and in vitro cytotoxicity evaluation of β-carboline-linked 2, 4-thiazolidinedione hybrids: Potential DNA intercalation and apoptosis inducing studies, New J. Chem. 42 (2018) 16226–16236;
(b) O.A. Pena-Moran, M.L. Villarreal, L. Alvarez-Berber, A. Meneses-Acosta, V. Rodriguez-Lopez, Cytotoxicity, post-treatment recovery, and selectivity analysis of naturally occurring podophyllotoxins from Bursera fagaroides var. fagaroides on breast cancer cell lines, Molecules 21 (2016) 1013–1027;
(c) G.d. Barrio, F. Parra, Evaluation of the antiviral activity of an aqueous extract from Phyllanthus Orbicularis, J. Ethnopharmacol. 72 (2000) 317–322.

[30] (a) C. Jadala, M. Sathish, T.S. Reddy, V.G. Reddy, R. Tokala, S.K. Bhargava, N. Shankaraiah, N. Nagesh, A. Kamal, Synthesis and in vitro cytotoxicity evaluation of β-carboline-combretastatin carboxamides as apoptosis inducing agents: DNA intercalation and topoisomerase-II inhibition, Bioorg. Med. Chem. 27 (2019) 3285–3298;
(b) L. Gardner, R. Malik, Y. Shimizu, N. Mullins, W.M. Elshamy, Geminin overexpression prevents the completion of topoisomerase IIα chromosome decatenation, leading to aneuploidy in human mammary epithelial cells, Breast Cancer Research 13 (2011) R53–R73;
(c) A. Kamal, N.S. Rao, N. Nagesh, L.V. Nayak, S. Sunkari, R. Tokala, G. Kiranmayi, P. Regur, N. Shankaraiah, Design and synthesis of DNA-intercalative naphthalimide- benzothiazole/cinnamide derivatives: cytotoxicity evaluation and topoisomerase-IIα inhibition, Med. chem. Commun. 10 (2019) 72–79.

[31] (a) M.A. Aleksic, V. Kapetanovic, An overview of the optical and electrochemical methods for detection of DNA-DNA interactions, Acta Chim. Slov. 61 (2014) 555–573;
(b) X. Shui, M.E. Peek, L.A. Lipscomb, Q. Gao, C. Ogata, B.P. Roques, C. Garbay-Jaureguiberry, A.P. Wilkinson, L.D. Wiliams, Effects of cationic charge on three-dimensional structures of intercalative complexes structure of a bis-intercalated DNA complex solved by MAD phasing, Curr. Med. Chem. 7 (2000) 59–71.

[32] (a) A.A. Phadte, S. Banerjee, N.A. Mate, A. Banerjee, Spectroscopic and viscometric determination of DNA-binding modes of some bioactive dibenzodioxins and phenazines, Biochem. Biophys. 18 (2019) 100629–100635;
(b) W. Bauer, J. Vinograd, The interaction of closed circular DNA with intercalative dyes: III, Dependency of the buoyant density upon superhelix density and base composition. 54 (1970) 281–298.

[33] R. Martinez, L. Chacon-Garcia, The search of DNA-intercalators as antitumoral drugs: what it worked and what did not work, Curr. Med. Chem 12 (2005) 127–151.
[34] S. Nekkanti, K. Veeramani, S.S. Kumari, R. Tokala, N. Shankaraiah, A recyclable and water soluble copper (I)-catalyst: one-pot synthesis of 1, 4-disubstituted 1, 2, 3-triazoles and their biological evaluation, RSC Adv. 6 (2017) 103556–103566.
[35] (a) S. Dasari, P.B. Tchounwou, Cisplatin in cancer therapy: molecular mechanisms of action, Eur. J. Pharmacol. (2014) 364–378;
(b) T. Kishimoto, Y. Yoshikawa, K. Yoshikawa, S. Komeda, Different effects of cisplatin and transplatin on the higher-order structure of DNA and gene expression, Int. J. Mol. Sci. 21 (2020) 34–48.
[36] R. Preet, B. Chakraborty, S. Siddharth, P. Mohapatra, D. Das, S.R. Satapathy, S. Das, N.C. Maiti, P.R. Maulik, C.N. Kundu, C. Chowdury, Synthesis and biological evaluation of andrographolide analogues as anti-cancer agents, Eur. J. Med. Chem. 85 (2014) 95–106.
[37] J. Gour, S. Gatadi, V. Pooladanda, S.M. Ghouse, S. Malasala, Y.V. Madhavi, C. Godugu, S. Nanduri, Facile synthesis of 1,2,3-triazole-fused indolo-and pyrrole [1,4]diazepines, DNA-binding and evaluation of their anticancer evaluation, Bioorg. Chem. 93 (2019) 103306–103320.
[38] G. Priyadarshini, S. Amrutkar, A. Nayak, U.C. Banerjee, C.N. Kundu, S.K. Guchhait, Scaffold-hopping of bioactive flavonoids: discovery of aryl-pyridopyrimidinones as potent anticancer agents that inhibit catalytic role of topoisomerase IIα, Eur. J. Med. Chem. 122 (2016) 43–54.
[39] S. Elmore, Apoptosis: a review of programmed cell death, Toxicol. Pathol. 35 (2007) 495–516.
[40] R. Tokala, S. Bale, I.P. Janrao, A. Vennela, N.P. Kumar, K.R. Senwar, C. Godugu, N. Shankaraiah, Synthesis of 1, 2, 4-triazole-linked urea/thiourea conjugates as cytotoxic and apoptosis inducing agents, Bioorg. Med. Chem. Lett. 28 (2018) 1919–1924.
[41] B. Tarnowski, F.G. Spinale, J.H. Nicholson, DAPI as a useful stain for nuclear quantification, Biotech. Histochem. 66 (1991) 297–302.
[42] (a) S.-H. Lee, X.W. Meng, K.S. Flatten, D.A. Loegering, S.H. Kaufmann, Phosphatidylserine exposure during apoptosis reflects bidirectional trafficking between plasma membrane and cytoplasm, Cell Death Differ. 20 (2013) 64–76;
(b) I. Vermes, C. Haanen, H. Steffens-Nakken, C. Reutellingsperger, A novel assay for apoptosis flow cytometric detection of phosphatidylserine expression on early apoptotic cells using fluorescein labelled annexin V, J. Immunol. Methods 184 (1995) 39–51.
[43] (a) J.M. Suski, M. Lebiedzinska, M. Bonora, P. Pinton, J. Duszynski, M. R. Wieckowski, Relation between mitochondrial membrane potential and ROS formation, Methods Mol. Biol. 1782 (2018) 357–381;
(b) F. Sivandzade, A. Bhalerao, L. Cucullo, Analysis of the mitochondrial membrane potential using the cationic JC-1 dye as a sensitive functional probe, Bio. Protoc. 9 (2019), e3128;
(c) M. Reers, S.T. Smiley, C. Mottola-Hartshorn, A. Chen, M. Lin, L.B. Chen, Mitochondrial membrane potential monitored by JC-1 dye, Methods Enzymol. 260 (1995) 406–417.
[44] T.A. Martin, L. Ye, A.J. Sanders, J. Lane, W.G. Jiang, Cancer invasion and metastasis: molecular and cellular perspective. Landes Bioscience; 2000–2013.
[45] (a) L.G. Rodriguez, X. Wu, J.L. Guan, Wound-healing assay, Methods Mol Biol. 294 (2005) 23–29;
(b) V.G. Reddy, T.S. Reddy, C. Jadala, M.S. Reddy, F. Sultana, R. Akunuri, S. K. Bhargava, D. Wlodkowic, P. Srihari, A. Kamal, Pyrazolo-benzothiazole hybrids: Synthesis, anticancer properties and evaluation of antiangiogenic activity using in vitro VEGF-2 kinase and in vivo transgenic zebrafish model, Eur. J. Med. Chem. 182 (2019) 111609–111623.
[46] A. Sethi, K. Joshi, K. Sasikala, M. Alvala, Molecular docking in modern drug discovery: principles and recent applications, Drug Discovery Develop. New Adv. (2019) 27–39.
[47] Y.R. Wang, S.F. Chen, C.C. Wu, Y.W. Liao, T.S. Lin, K.T. Liu, Y.S. Chen, T.K. Li, T. C. Chien, N.L. Chan, Producing irreversible topoisomerase II-mediated DNA breaks by site-specific Pt(II)-methionine coordination chemistry, Nucleic Acids Res. 45 (2017) 10861–10871.
[48] Schrödinger suite 2017-1, (2017) Schrödinger, LLC, New York, NY, 2017.
[49] S. Sana, V.G. Reddy, S. Bhandari, T.S. Reddy, R. Tokala, A.P. Sakla, S.K. Bhargava, N. Shankaraiah, Exploration of carbamide derived pyrimidine-thioindole conjugates as potential VEGFR-2 inhibitors with anti-angiogenesis effect, Eur. J. Med. Chem. 200 (2020) 112457–112478.
[50] C.A. Lipinski, Lead- and drug-like compounds: the rule-of-five revolution, Drug Discov. Today Technol. 1 (2004) 337–341.
[51] S.P. Khathi, B. Chandrasekaran, S. Karunanidhi, C.L. Tham, F. Kozielski, N. Sayyad, R. Karpoormath, Design and synthesis of novel thiadiazole-thiazolone hybrids as potential inhibitors of the human mitotic kinesin Eg5, Bioorg. Med. Chem. Lett. 28 (2018) 2930–2938.
[52] F. Cheng, W. Li, G. Liu, Y. Tang, In silico ADMET prediction: recent advances, current challenges and future trends, Curr. Top. Med. Chem. 13 (2013) 1273–1289.
[53] Qikprop (Version 5.1). (2017-1): Schrödinger, LLC, New York, NY, 2017.
[54] K. Enslein, V.K. Gombar, B.W. Blake, International Commission for Protection Against Environmental Mutagens and Carcinogens. Use of SAR in computer-assisted prediction of carcinogenicity and mutagenicity of chemicals by the TOPKAT program, Mutation Res. 305 (1994) 47–61.
[55] J. Dearden, In silico prediction of drug toxicity, J. Comput.-Aided Mol. Des. 17 (2003) 119.
[56] A.M. Rieger, K.L. Nelson, J.D. Konowalchuk, D.R. Barreda, Modified annexin V/ propidium iodide apoptosis assay for accurate assessment of cell death, J Vis. Exp. 50 (2011) 2597.